The Air Pollution Model (TAPM) Version 3. Part 1: Technical Description

Peter J. Hurley

Atmospheric Research
CSIRO Atmospheric Research Technical Paper 71

The Air Pollution Model (TAPM) Version 3. Part 1: Technical Description

Peter J. Hurley

CSIRO Atmospheric Research Technical Paper No. 71

National Library of Cataloguing-in-Publication entry

Hurley, Peter, 1963- .

The air pollution model (TAPM) version 3. Part 1, Technical description.

ISBN 0 643 06891 0.

1. Air - Pollution - Mathematical models. 2. Air - Pollution - Measurement. 3. Air - Pollution - Meteorological aspects. I. CSIRO. Division of Atmospheric Research. II. Title. (Series : CSIRO Atmospheric Research technical paper (Online) ; 71).

363.7392

Address and contact details: CSIRO Atmospheric Research
Private Bag No. 1 Aspendale Victoria 3195 Australia
Ph: (+61 3) 9239 4400; fax: (+61 3) 9239 4444
e-mail: ar-enquiries@csiro.au

CSIRO Atmospheric Research Technical Papers may be issued out of sequence. From July 2000 All new Technical Papers will appear on the web site of CSIRO Atmospheric Research. Some Technical Papers will also appear in paper form.

The Air Pollution Model (TAPM) Version 3. Part 1: Technical Description

Peter J. Hurley
CSIRO Atmospheric Research
Private Bag 1, Aspendale,
Vic 3195, Australia

Abstract

Air pollution predictions for environmental impact assessments usually use Gaussian plume/puff models driven by observationally-based meteorological inputs. An alternative approach is to use prognostic meteorological and air pollution models, which have many advantages over the Gaussian approach and are now a viable tool for performing year-long simulations. This report provides a comprehensive technical description of the newly enhanced prognostic model called The Air Pollution Model (TAPM).

1 Introduction

Air pollution models that can be used to predict hour by hour pollution concentrations for periods of up to a year, are generally semi-empirical/analytic approaches based on Gaussian plumes or puffs. These models typically use either a simple surface based meteorological file or a diagnostic wind field model based on available observations. The Air Pollution Model (TAPM) is different to these approaches in that it solves approximations to the fundamental fluid dynamics and scalar transport equations to predict meteorology and pollutant concentration for a range of pollutants important for air pollution applications. TAPM consists of coupled prognostic meteorological and air pollution concentration components, eliminating the need to have site-specific meteorological observations. Instead, the model predicts the flows important to local-scale air pollution, such as sea breezes and terrain-induced flows, against a background of larger-scale meteorology provided by synoptic analyses.

The meteorological component of TAPM is an incompressible, non-hydrostatic, primitive equation model with a terrain-following vertical coordinate for three-dimensional simulations. The model solves the momentum equations for horizontal wind components, the incompressible continuity equation for vertical velocity, and scalar equations for potential virtual temperature and specific humidity of water vapour, cloud water/ice, rain water and snow. The Exner pressure function is split into hydrostatic and non-hydrostatic components, and a Poisson equation is solved for the non-hydrostatic component. Explicit cloud micro-physical processes are included. The turbulence terms in these equations have been determined by solving equations for turbulence kinetic energy and eddy dissipation rate, and then using these values in representing the vertical fluxes by a gradient diffusion approach, including a counter-gradient term for heat flux. A vegetative canopy, soil scheme, and urban scheme are used at the surface, while radiative fluxes, both at the surface and at upper levels, are also included.

The air pollution component of TAPM, which uses the predicted meteorology and turbulence from the meteorological component, consists of four modules. The Eulerian Grid Module (EGM) solves prognostic equations for the mean and variance of concentration, and for the cross-correlation of concentration and virtual potential temperature. The Lagrangian Particle Module (LPM) can be used to represent near-source dispersion more accurately. The Plume Rise Module is used to account for plume momentum and buoyancy effects for point sources. The Building Wake Module allows plume rise and dispersion to include wake effects on meteorology and turbulence. The model also includes gas-phase photochemical reactions based on the Generic Reaction Set, gas- and aqueous-phase chemical reactions for sulfur dioxide and particles, and a dust mode for total suspended particles ($PM_{2.5}$, PM_{10}, PM_{20} and PM_{30}). Wet and dry deposition effects are also included.

This paper describes the technical details of the modelling approach, including the meteorological component in Section 2 and the pollution component in Section 3. Section 4 outlines the numerical methods used in the model. Changes in TAPM V3.0 from the previous major release of the model (V2.0) are summarised in the Appendix. Part 2 of this paper (Hurley et al., 2005) presents a summary of some verification studies performed with TAPM V3.0.

2 Meteorological component

The meteorological component of TAPM is an incompressible, optionally non-hydrostatic, primitive equation model with a terrain-following vertical coordinate for three-dimensional simulations. It includes parameterisations for cloud/rain/snow micro-physical processes, turbulence closure, urban/vegetative canopy and soil, and radiative fluxes. The model solution for winds, potential virtual temperature and specific humidity, is weakly nudged with a 24-hour e-folding time towards the synoptic-scale input values of these variables.

Note that the horizontal model domain size should be restricted in size to less than about 1500 km x 1500 km, as the model equations neglect the curvature of the earth and assume a uniform distance grid spacing across the domain.

2.1 Base meteorological variables

The mean wind is determined for the horizontal components u and v (m s^{-1}) from the momentum equations and the terrain following vertical velocity $\dot{\sigma}$ (m s^{-1}) from the continuity equation. Potential virtual temperature θ_v (K) is determined from an equation combining conservation of heat and water vapour. The Exner pressure function $\pi = \pi_H + \pi_N$ (J kg^{-1} K^{-1}) is determined from the sum of the hydrostatic component π_H and non-hydrostatic component π_N (see Section 2.2). The equations for these variables are as follows

$$\frac{du}{dt} = \frac{\partial}{\partial x}\left(K_H \frac{\partial u}{\partial x}\right) + \frac{\partial}{\partial y}\left(K_H \frac{\partial u}{\partial y}\right) - \frac{\partial \overline{w'u'}}{\partial \sigma}\frac{\partial \sigma}{\partial z} - \theta_v\left(\frac{\partial \pi}{\partial x} + \frac{\partial \pi}{\partial \sigma}\frac{\partial \sigma}{\partial x}\right) + fv + F(u) - N_s(u - u_s) \quad (1)$$

$$\frac{dv}{dt} = \frac{\partial}{\partial x}\left(K_H \frac{\partial v}{\partial x}\right) + \frac{\partial}{\partial y}\left(K_H \frac{\partial v}{\partial y}\right) - \frac{\partial \overline{w'v'}}{\partial \sigma}\frac{\partial \sigma}{\partial z} - \theta_v\left(\frac{\partial \pi}{\partial y} + \frac{\partial \pi}{\partial \sigma}\frac{\partial \sigma}{\partial y}\right) - fu + F(v) - N_s(v - v_s) \quad (2)$$

$$\frac{\partial \dot{\sigma}}{\partial \sigma} = -\left(\frac{\partial u}{\partial x} + \frac{\partial v}{\partial y}\right) + u\frac{\partial}{\partial \sigma}\left(\frac{\partial \sigma}{\partial x}\right) + v\frac{\partial}{\partial \sigma}\left(\frac{\partial \sigma}{\partial y}\right) \quad (3)$$

$$\frac{d\theta_v}{dt} = \frac{\partial}{\partial x}\left(K_H \frac{\partial \theta_v}{\partial x}\right) + \frac{\partial}{\partial y}\left(K_H \frac{\partial \theta_v}{\partial y}\right) - \frac{\partial \overline{w'\theta_v'}}{\partial \sigma}\frac{\partial \sigma}{\partial z} + S_{\theta_v} + F(\theta_v) - N_s(\theta_v - \theta_{vs}) \quad (4)$$

$$\frac{\partial \pi_H}{\partial \sigma} = -\frac{g}{\theta_v}\left(\frac{\partial \sigma}{\partial z}\right)^{-1} \quad (5)$$

where

t = time (s),

x, y, σ = the components of the coordinate system (m),

$\sigma = z_T\left(\frac{z - z_s}{z_T - z_s}\right)$,

z = cartesian vertical coordinate (m),

z_T = height of model top (m),

z_s = terrain height (m),

$\frac{d\phi}{dt} \equiv \frac{\partial \phi}{\partial t} + u\frac{\partial \phi}{\partial x} + v\frac{\partial \phi}{\partial y} + \dot{\sigma}\frac{\partial \phi}{\partial \sigma}$,

K_H = horizontal diffusion coefficient (see Section 2.4),

$\overline{w'\phi'}$ = vertical flux of ϕ (see Section 2.4),

$F(\phi)$ = horizontal filtering of ϕ (see Section 4.3),

f = Coriolis parameter ($4\pi_c \sin(lat)/(24 \times 3600)$) ($s^{-1}$),

π_c = 3.14159265,

lat = latitude (^{o}),

u_s, v_s, θ_{vs} = large scale synoptic winds and potential virtual temperature,

N_s = large scale nudging coefficient ($1/(24 \times 3600)$),

$S_{\theta_v} = \frac{\theta_v}{T}\left(\frac{\partial T}{\partial t}\right)_{RADIATION} - \frac{\lambda}{c_p} S_{q_V}$ (see Sections 2.3 and 2.5),

T = temperature (K),

g = gravitational constant (9.81 m s^{-2}),

λ = latent heat of vaporisation of water (2.5×10^6 J kg^{-1}),

c_p = specific heat at constant pressure (1006 J kg^{-1} K^{-1}),

$\frac{\partial \sigma}{\partial x} = \left(\frac{\sigma - z_T}{z_T - z_s}\right)\frac{\partial z_s}{\partial x}$, $\frac{\partial \sigma}{\partial y} = \left(\frac{\sigma - z_T}{z_T - z_s}\right)\frac{\partial z_s}{\partial y}$, $\frac{\partial \sigma}{\partial z} = \left(\frac{z_T}{z_T - z_s}\right)$.

2.2 Non-hydrostatic pressure

The optional non-hydrostatic component of the Exner pressure function π_N is determined by taking spatial derivatives of the three momentum equations and the time derivative of the continuity equation, and then eliminating all time derivatives in the continuity equation by substitution. The following assumes all products of Coriolis terms and terrain gradients, and all turbulence and synoptic variation terms, can be neglected. The resultant equation for π_N is

$$\frac{\partial^2 \pi_N}{\partial x^2} + 2\frac{\partial \sigma}{\partial x}\frac{\partial^2 \pi_N}{\partial x \partial \sigma} + \frac{\partial^2 \pi_N}{\partial y^2} + 2\frac{\partial \sigma}{\partial y}\frac{\partial^2 \pi_N}{\partial y \partial \sigma} + \left(\frac{\partial \sigma}{\partial z}\right)^2 \frac{\partial^2 \pi_N}{\partial \sigma^2} + C_x \frac{\partial \pi_N}{\partial x} + C_y \frac{\partial \pi_N}{\partial y} + C_\sigma \frac{\partial \pi_N}{\partial \sigma} = R_\pi, \quad (6)$$

with coefficients

$$C_x = \frac{1}{\theta_v}\left(\frac{\partial \theta_v}{\partial x} + \frac{\partial \theta_v}{\partial \sigma}\frac{\partial \sigma}{\partial x}\right),\ C_y = \frac{1}{\theta_v}\left(\frac{\partial \theta_v}{\partial y} + \frac{\partial \theta_v}{\partial \sigma}\frac{\partial \sigma}{\partial y}\right),$$

$$C_\sigma = \frac{1}{\theta_v}\left(\frac{\partial \theta_v}{\partial x}\frac{\partial \sigma}{\partial x} + \frac{\partial \theta_v}{\partial y}\frac{\partial \sigma}{\partial y} + \frac{\partial \theta_v}{\partial \sigma}\left(\frac{\partial \sigma}{\partial z}\right)^2\right) + \frac{\partial^2 \sigma}{\partial x^2} + \frac{\partial^2 \sigma}{\partial y^2},$$

$$R_\pi = \frac{1}{\theta_v}\left(\frac{\partial R_u}{\partial x} + \frac{\partial R_v}{\partial y} + \frac{\partial R_{\dot\sigma}}{\partial \sigma} - R_u \frac{\partial}{\partial \sigma}\left(\frac{\partial \sigma}{\partial x}\right) - R_v \frac{\partial}{\partial \sigma}\left(\frac{\partial \sigma}{\partial y}\right)\right),$$

$$R_u = -u\frac{\partial u}{\partial x} - v\frac{\partial u}{\partial y} - \dot\sigma\frac{\partial u}{\partial \sigma} + fv - \theta_v \frac{\partial \pi_H}{\partial x} + g\frac{\partial \sigma}{\partial x}\left(\frac{\partial \sigma}{\partial z}\right)^{-1},$$

$$R_v = -u\frac{\partial v}{\partial x} - v\frac{\partial v}{\partial y} - \dot\sigma\frac{\partial v}{\partial \sigma} - fu - \theta_v \frac{\partial \pi_H}{\partial y} + g\frac{\partial \sigma}{\partial y}\left(\frac{\partial \sigma}{\partial z}\right)^{-1},$$

$$R_{\dot\sigma} = -u\frac{\partial \dot\sigma}{\partial x} - v\frac{\partial \dot\sigma}{\partial y} - \dot\sigma\frac{\partial \dot\sigma}{\partial \sigma} - \theta_v\left(\frac{\partial \pi_H}{\partial x}\frac{\partial \sigma}{\partial x} + \frac{\partial \pi_H}{\partial y}\frac{\partial \sigma}{\partial y}\right) + u^2\frac{\partial^2 \sigma}{\partial x^2} + 2uv\frac{\partial^2 \sigma}{\partial x \partial y} + v^2\frac{\partial^2 \sigma}{\partial y^2} + 2\dot\sigma\left(u\frac{\partial}{\partial \sigma}\left(\frac{\partial \sigma}{\partial x}\right) + v\frac{\partial}{\partial \sigma}\left(\frac{\partial \sigma}{\partial y}\right)\right),$$

and

$$\frac{\partial}{\partial \sigma}\left(\frac{\partial \sigma}{\partial x}\right) = \left(\frac{1}{z_T - z_s}\right)\frac{\partial z_s}{\partial x},\ \frac{\partial}{\partial \sigma}\left(\frac{\partial \sigma}{\partial y}\right) = \left(\frac{1}{z_T - z_s}\right)\frac{\partial z_s}{\partial y},$$

$$\frac{\partial^2 \sigma}{\partial x^2} = \left(\frac{\sigma - z_T}{z_T - z_s}\right)\frac{\partial^2 z_s}{\partial x^2},\ \frac{\partial^2 \sigma}{\partial x \partial y} = \left(\frac{\sigma - z_T}{z_T - z_s}\right)\frac{\partial^2 z_s}{\partial x \partial y},\ \frac{\partial^2 \sigma}{\partial y^2} = \left(\frac{\sigma - z_T}{z_T - z_s}\right)\frac{\partial^2 z_s}{\partial y^2}.$$

2.3 Water and ice micro-physics

Conservation equations are solved for specific humidity (kg kg^{-1}) $q = q_V + q_C + q_I$ (representing the sum of water vapour, cloud water and cloud ice respectively), specific humidity (kg kg^{-1}) of rain water q_R and specific humidity (kg kg^{-1}) of snow q_S:

$$\frac{dq}{dt} = \frac{\partial}{\partial x}\left(K_H \frac{\partial q}{\partial x}\right) + \frac{\partial}{\partial y}\left(K_H \frac{\partial q}{\partial y}\right) - \frac{\partial \overline{w'q'}}{\partial \sigma}\frac{\partial \sigma}{\partial z} + S_{q_V} + S_{q_C} + S_{q_I} - N_{syn}\left(q - q_{syn}\right)$$

$$\frac{dq_R}{dt} = \frac{\partial}{\partial x}\left(K_H \frac{\partial q_R}{\partial x}\right) + \frac{\partial}{\partial y}\left(K_H \frac{\partial q_R}{\partial y}\right) - \frac{\partial \overline{w'q'_R}}{\partial \sigma}\frac{\partial \sigma}{\partial z} + S_{q_R} - \mathrm{V_{TR}}\frac{\partial q_R}{\partial \sigma}\frac{\partial \sigma}{\partial z}$$

$$\frac{dq_S}{dt} = \frac{\partial}{\partial x}\left(K_H \frac{\partial q_S}{\partial x}\right) + \frac{\partial}{\partial y}\left(K_H \frac{\partial q_S}{\partial y}\right) - \frac{\partial \overline{w'q'_S}}{\partial \sigma}\frac{\partial \sigma}{\partial z} + S_{q_S} - \mathrm{V_{TS}}\frac{\partial q_S}{\partial \sigma}\frac{\partial \sigma}{\partial z}$$

with

$S_{q_V}, S_{q_C}, S_{q_I}, S_{q_R}, S_{q_S}$ = micro - physical source terms,

q_{syn} = synoptic scale specific humidity of water vapour plus cloud water/ice,

$\mathrm{V}_{TR}, \mathrm{V}_{TS}$ = terminal velocity of rain/snow,

and the specific humidity of water vapour q_V and the saturated specific humidity q_{VS} determined from

$$q_V = \min(q, q_{VS}),$$

$$q_{VS} = \frac{0.622 e_{VS}}{(p - 0.378 e_{VS})},$$

p = pressure (Pa), and

$$e_{VS} = 610 \exp\left(\frac{\lambda}{R_v} \left(\frac{1}{273.15} - \frac{1}{T} \right) \right),$$

$$\lambda = \begin{cases} \mathrm{L_V}, & \text{if } T \geq 273.15 \\ \mathrm{L_S}, & \text{if } T < 273.15 \end{cases}.$$

Cloud water and cloud ice are assumed to co-exist only between temperatures of –15°C and 0°C, with a linear relationship used between these two limits (see Rotstayn (1997) for a discussion of mixed-phase clouds):

$$q_C = \left(1 + \left(\frac{T - 273.15}{15} \right) \right) (q - q_V),$$

$$q_I = q - q_V - q_C.$$

The source terms in the conservation equations are

$$S_{q_V} = -P_{VC} - P_{VI} - P_{VR} - P_{VS},$$

$$S_{q_C} = P_{VC} - P_{CI} - P_{CR} - P_{CS},$$

$$S_{q_I} = P_{VI} + P_{CI} - P_{IR} - P_{IS},$$

$$S_{q_R} = P_{VR} + P_{CR} + P_{IR} - P_{RS},$$

$$S_{q_S} = P_{VS} + P_{CS} + P_{IS} + P_{RS}.$$

Bulk parameterisations of the micro-physics are based mainly on Tripoli and Cotton (1980) and Lin et al. (1983), with some updated constants/parameterisations as used by Katzfey and Ryan (1997), Rotstayn (1997) and Ryan (2002). The micro-physical production terms used here are as follows:

$$P_{VC} = \left(\frac{q_V - q_{VS}}{\Delta t} \right) \left(1 + \frac{L_V}{c_p} \frac{dq_{VS}}{dT} \right)^{-1}$$

$$P_{VI} = \left(\frac{q_V - q_{VS}}{\Delta t} \right) \left(1 + \frac{L_S}{c_p} \frac{dq_{VS}}{dT} \right)^{-1}$$

$$P_{CI} = 0$$

$$P_{IR} = 0$$

$$P_{CR} = P_{CR1} + P_{CR2}$$

$$P_{CR1} = \frac{0.104 E_{CR1} g}{\mu} H(q_C - q_{C0}) \left(\frac{\rho^4 q_C^7}{N_C \rho_W} \right)^{1/3}$$

$$P_{CR2} = \frac{\pi}{4} E_{CR2} a_R N_{R0} \Gamma(3.5) \left(\frac{\rho}{\rho_0} \right)^{1/2} q_C \lambda_R^{-3.5}$$

$$P_{CS} = \frac{\pi}{4} E_{CS} a_S N_{S0} \Gamma(3.25) \left(\frac{\rho}{\rho_0} \right)^{1/2} q_C \lambda_S^{-3.25}$$

$$P_{IS} = P_{IS1} + P_{IS2}$$

$$P_{IS1} = 0.005 E_{IS} (q_I - q_{I0}) H(q_I - q_{I0})$$

$$P_{IS2} = \frac{\pi}{4} E_{IS} a_S N_{S0} \Gamma(3.25) \left(\frac{\rho}{\rho_0} \right)^{1/2} q_I \lambda_S^{-3.25}$$

$$P_{VR} = \min(0, \frac{q_V}{q_{VS}} - 1) \frac{q_R \lambda_R^2}{\rho_W} \left(\frac{0.5 + \frac{0.349}{\mu^{1/2}} \left(\frac{\rho_W g \rho}{\lambda_R^3} \right)^{1/4}}{\frac{L_V^2}{K R_V T^2} + \frac{R_V T}{e_{VS} D_V}} \right)$$

$$P_{VS} = \frac{2\pi}{\rho} \min(0, \frac{q_V}{q_{VS}} - 1) \left(\frac{\frac{0.78}{\lambda_S^2} + \frac{0.31 \Gamma(2.625) a_S^{1/2}}{\nu^{1/2} \lambda_S^{2.625}} \left(\frac{\rho_0}{\rho} \right)^{1/4}}{\frac{L_S^2}{K R_V T^2} + \frac{R_V T}{e_{VS} D_V}} \right)$$

$P_{RS} = -q_S / \Delta t$ if $T > 275.15$.

where H is the Heaviside function,

$$\lambda_R = \left(\frac{\pi \rho_R N_{R0}}{\rho q_R} \right)^{1/4}, \ \lambda_S = \left(\frac{\pi \rho_S N_{S0}}{\rho q_S} \right)^{1/4},$$

$a_R = 141.5, \ a_S = 4.84,$

$q_{C0} = \frac{4}{3} \pi \rho_W r_C^3 N_C \rho^{-1},$

$$q_{CI} = \begin{cases} \rho 2.316 \times 10^{(-6.0 - 0.0413(T - 273.15))}, & \text{if } T > 255.65 \\ \rho 1.158 \times 10^{(-4.0 + 0.0519(T - 273.15))}, & \text{otherwise} \end{cases},$$

$E_{CR1} = 0.55, \ E_{CR2} = 0.7, \ E_{CS} = 0.7, \ E_{IS} = \exp(0.025(T - 273.15)).$

Other constants are

$L_V = 2.5\times10^6$ J kg^{-1}, $L_S = 2.83\times10^6$ J kg^{-1},
$N_C = 3\times10^8$ m^{-3}, $r_{C0} = 1\times10^{-5}$ m, $N_{R0} = 8\times10^6$ m^{-4}, $N_{S0} = 3\times10^6$ m^{-4},
$\rho_W = 1000$ kg m^{-3}, $\rho_S = 100$ kg m^{-3}, $R_V = 461.5$ J kg^{-1} K^{-1},
$\mu = 1.8\times10^{-5}$ kg m^{-1} s^{-1}, $\nu = 1.35\times10^{-5}$ m^2 s^{-1},
$K = 0.025$ J m^{-1} s^{-1}, $D_V = 2.5\times10^{-5}$ m^2 s^{-1}.

The rain/snow terminal velocity is determined from

$$V_{TR} = -\frac{a_R\Gamma(4.5)}{6\lambda_R^{0.5}}\left(\frac{\rho_0}{\rho}\right)^{1/2},$$

$$V_{TS} = -\frac{a_S\Gamma(4.25)}{6\lambda_S^{0.25}}\left(\frac{\rho_0}{\rho}\right)^{1/2}.$$

Calculation of the precipitation rate (m s^{-1}) at the surface is from $P = \frac{\rho}{\rho_W}V_{TR}q_R(0)$, where $q_R(0)$ is the amount of rain reaching the ground, and similarly for snowfall, but using snow density, terminal velocity and specific humidity.

In order to account for the lack of cloud water information in the synoptic analyses, we enhance the synoptic total water used in the model, by enhancing the synoptic-scale specific humidity:

$$q_{enhanced} = \max\left(q_{synoptic}, 2q_{synoptic} - q_{sat}RH_C/100\right),$$

where $q_{synoptic}$ is the original synoptic-scale specific humidity and RH_C = 85% is the threshold value above which enhancement is carried out. This parameterisation results in no change to the synoptic-scale relative humidity for $RH_{synoptic} < RH_C$ and gives an enhanced value of 100% when $RH_{synoptic}$ = 92.5%. This approach is consistent with cloud cover parameterisations used in global and synoptic scale models.

2.4 Turbulence and diffusion

Turbulence closure in the mean equations uses a gradient diffusion approach, which depends on a diffusion coefficient *K* and gradients of mean variables. Using Cartesian tensor notation, the fluxes are

$$\overline{u_i'u_j'} = \frac{2}{3}E\delta_{ij} - K\left(\frac{\partial u_i}{\partial x_j} + \frac{\partial u_j}{\partial x_i}\right),$$

$$\overline{u_i'\theta_v'} = -K\left(\frac{\partial\theta_v}{\partial x_i} - \gamma_{\theta_v}\right),$$

$$\overline{u_i'\phi'} = -2.5K\frac{\partial\phi}{\partial x_i},$$

where

i, j are subscripts for the three coordinate directions (i.e. $i = 1,2,3$ for x,y,z respectively),

u_i, u_j represent velocities,

$\delta_{ij} = \begin{cases} 1 \text{ if } i = j, \\ 0 \text{ otherwise.} \end{cases}$

$\gamma_{\theta_v} = 0.00065 \text{ K m}^{-1}$ from Deardorff (1966),

ϕ represents a scalar.

The scalar diffusion coefficient of 2.5 used above is based on an analysis of the second order closure equations from Andren (1990), with constants from Rodi (1985).

The turbulence scheme used to calculate K is the standard E-ε model in three-dimensional terrain-following coordinates, with constants for the eddy dissipation rate equation derived from the analysis of Duynkerke (1988). The model solves prognostic equations for the turbulence kinetic energy (E) and the eddy dissipation rate (ε)

$$\frac{dE}{dt} = \frac{\partial}{\partial x}\left(K_H \frac{\partial E}{\partial x}\right) + \frac{\partial}{\partial y}\left(K_H \frac{\partial E}{\partial y}\right) + \left(\frac{\partial \sigma}{\partial z}\right)^2 \frac{\partial}{\partial \sigma}\left(K \frac{\partial E}{\partial \sigma}\right) + P_s + P_b - \varepsilon, \tag{9}$$

$$\frac{d\varepsilon}{dt} = \frac{\partial}{\partial x}\left(K_H \frac{\partial \varepsilon}{\partial x}\right) + \frac{\partial}{\partial y}\left(K_H \frac{\partial \varepsilon}{\partial y}\right) + \left(\frac{\partial \sigma}{\partial z}\right)^2 \frac{\partial}{\partial \sigma}\left(c_{\varepsilon 0} K \frac{\partial \varepsilon}{\partial \sigma}\right) + \frac{\varepsilon}{E}(c_{\varepsilon 1} \max(P_s, P_s + P_b) - c_{\varepsilon 2}\varepsilon), \tag{10}$$

where

$$P_s = 2K\left(\left(\frac{\partial u}{\partial x} + \frac{\partial u}{\partial \sigma}\frac{\partial \sigma}{\partial x}\right)^2 + \left(\frac{\partial v}{\partial y} + \frac{\partial v}{\partial \sigma}\frac{\partial \sigma}{\partial y}\right)^2 + \left(\frac{\partial w}{\partial \sigma}\frac{\partial \sigma}{\partial z}\right)^2\right) + K\left(\left(\frac{\partial u}{\partial y} + \frac{\partial u}{\partial \sigma}\frac{\partial \sigma}{\partial y} + \frac{\partial v}{\partial x} + \frac{\partial v}{\partial \sigma}\frac{\partial \sigma}{\partial x}\right)^2\right) + K\left(\left(\frac{\partial u}{\partial \sigma}\frac{\partial \sigma}{\partial z} + \frac{\partial w}{\partial x} + \frac{\partial w}{\partial \sigma}\frac{\partial \sigma}{\partial x}\right)^2 + \left(\frac{\partial v}{\partial \sigma}\frac{\partial \sigma}{\partial z} + \frac{\partial w}{\partial y} + \frac{\partial w}{\partial \sigma}\frac{\partial \sigma}{\partial y}\right)^2\right),$$

$$P_b = -\frac{g}{\theta_v} K\left(\frac{\partial \theta_v}{\partial \sigma}\frac{\partial \sigma}{\partial z} - \gamma_{\theta_v}\right),$$

with $w = \left(\frac{\partial \sigma}{\partial z}\right)^{-1}\left(\dot{\sigma} - u\frac{\partial \sigma}{\partial x} - v\frac{\partial \sigma}{\partial y}\right)$,

and $K_H = \max(10, K)$, $K = c_m \frac{E^2}{\varepsilon}$, $c_m = 0.09$, $c_{\varepsilon 0} = 0.69$, $c_{\varepsilon 1} = 1.46$, and $c_{\varepsilon 2} = 1.83$.

As an alternative to Equation (10) the model has an option to use a diagnostic eddy dissipation rate based on Duynkerke and Driedonks (1987). In this approach,

$$\varepsilon = c_m^{3/4}\frac{E^{3/2}}{l},$$

$$l = \min(l_b, l_s),$$

$$l_b = \left(\frac{\phi_M}{kz} + \frac{1}{l_o}\right)^{-1},$$

$$l_s = 0.36E^{1/2}\left(\frac{g}{\theta_v}\frac{\partial\theta_v}{\partial z}\right)^{-1/2},$$

$$l_o = 0.3\frac{\int Ezdz}{\int Edz},$$

ϕ_M = surface layer similarity function (see Section 2.6.4),

k = von Karman constant (0.4).

Turbulence kinetic energy and eddy dissipation rate are enhanced in the top-half of the convective boundary layer (CBL), where turbulence levels can be underestimated using the above approaches. This has been achieved by using a simple parameterisation that limits the rate of decrease of prognostic turbulence with height, between heights in the range 0.55–0.95 times the CBL height, provided that the height is above the surface layer and the convective velocity scale is greater than 0.5 m s^{-1}.

2.5 Radiation

2.5.1 Clear-sky

Radiation at the surface is used for the computation of surface boundary conditions and scaling variables (see later), with the clear-sky incoming short-wave component from Mahrer and Pielke (1977),

$$R^{in}_{sw(clear-sky)} = \begin{cases}(a_g - a_w(z_s))S_{\text{Slope}}S_o\cos\chi; & \text{for } \cos\chi > 0\\ 0; & \text{for } \cos\chi \le 0\end{cases},$$

and the clear-sky incoming long-wave component from Dilley and O'Brien (1999),

$$R^{in}_{lw(clear-sky)} = \left(59.38 + 113.7\left(\frac{T(\sigma_1)}{273.15}\right)^6 + 96.96\left(\frac{r(\sigma_1)}{25}\right)^{1/2}\right)\cos\alpha,$$

with

$$a_g = 0.485 + 0.515\left(1.014 - 0.16/\sqrt{\cos\chi}\right),$$

$$a_w(\sigma) = 0.039\left(\frac{r(\sigma)}{\cos\chi}\right)^{0.3},$$

$r(\sigma) = \int_{\sigma}^{z_T}\rho q d\sigma$ is the column water vapour amount (kg m^{-2} or mm) between z_T and σ,

χ is the zenith angle, and S_o is the solar constant (1367 W m^{-2}).

The solar declination, zenith, and terrain slope angles are calculated using

$$\sin\delta_s = \sin\left(23.5\pi_c/180\right)\sin\left(2\pi_c\, day/365\right),$$

$$\cos\chi = \cos(lat)\cos\delta_s\cos\left(\pi_c\left(hour-12\right)/12\right)+\sin(lat)\sin\delta_s,$$

$$S_{\text{Slope}} = \frac{\cos i}{\cos\chi}, \quad \cos i = \cos\alpha\cos\chi + \sin\alpha\sin\chi\cos(\beta-\eta),$$

$$\alpha = \tan^{-1}\left(\left(\frac{\partial z_s}{\partial x}\right)^2+\left(\frac{\partial z_s}{\partial y}\right)^2\right), \quad \eta = \tan^{-1}\left(\left(\frac{\partial z_s}{\partial y}\right)\left(\frac{\partial z_s}{\partial x}\right)^{-1}\right)-\frac{\pi_c}{2},$$

$$\beta = \sin^{-1}\left(\cos\delta_s\sin\left(\pi_c\left(hour-12\right)/12\right)/\sin\chi\right),$$

lat = latitude, day = day of year ($1 \equiv 21$ March),

$hour$ = hour of day (24 hour clock), $\pi_c = 3.14159265$.

The effects of water vapour and carbon dioxide on atmospheric heating/cooling rates for both short-wave and long-wave radiation follow Mahrer and Pielke (1977)

$$\left.\frac{\partial T}{\partial t}\right|_{RADIATION\,(clear-sky)} = \frac{1}{\rho c_p}\left(-S_o\cos\chi\frac{\partial a_w}{\partial\sigma}\frac{\partial\sigma}{\partial z}\right.$$
$$\left.-\sigma_{SB}\frac{\partial\varepsilon\uparrow}{\partial\sigma}\frac{\partial\sigma}{\partial z}\left(\left(T(\sigma)\right)^4-\left(T(0)\right)^4\right)-\sigma_{SB}\frac{\partial\varepsilon\downarrow}{\partial\sigma}\frac{\partial\sigma}{\partial z}\left(\left(T(z_T)\right)^4-\left(T(\sigma)\right)^4\right)\right),$$

with

$$a_w(\sigma) = 0.039\left(\frac{r(\sigma)}{\cos\chi}\right)^{0.3},$$

$$r(\sigma) = \int_{\sigma}^{z_T}\rho q_v\, d\sigma,$$

and emissivity $\varepsilon = \varepsilon_{q_v}+\varepsilon_{CO_2}$ either integrated upwards $(\varepsilon\uparrow)$ or downwards $(\varepsilon\downarrow)$ with

$$\varepsilon_{q_v} = \begin{cases} 0.113\log_{10}\left(1+12.6\delta P\right), & \text{for } \log_{10}\delta P \le -4 \\ 0.104\log_{10}\delta P + 0.440, & \text{for } -4 < \log_{10}\delta P \le -3 \\ 0.121\log_{10}\delta P + 0.491, & \text{for } -3 < \log_{10}\delta P \le -1.5 \\ 0.146\log_{10}\delta P + 0.527, & \text{for } -1.5 < \log_{10}\delta P \le -1 \\ 0.161\log_{10}\delta P + 0.542, & \text{for } -1 < \log_{10}\delta P \le 0 \\ 0.136\log_{10}\delta P + 0.542, & \text{for } \log_{10}\delta P > 0 \end{cases},$$

$$\varepsilon_{CO_2} = 0.185\left(1-\exp\left(-0.39\left(\delta H\right)^{0.4}\right)\right),$$

$$\delta P = 0.1r(\sigma) = \begin{cases} 0.1\int_{z_S}^{\sigma}\rho q_v\, d\sigma, & \text{for } \varepsilon\uparrow \\ 0.1\int_{\sigma}^{z_T}\rho q_v\, d\sigma, & \text{for } \varepsilon\downarrow \end{cases},$$

$$\delta H = \begin{cases} 0.252\left(p_S - p\right)/100, & \text{for } \varepsilon\uparrow \\ 0.252\left(p - p_T\right)/100, & \text{for } \varepsilon\downarrow \end{cases},$$

where

p is pressure (hPa),

subscripts S and T indicate the ground surface or model top respectively,

and $\sigma_{SB} = 5.67 \times 10^{8}$ W m^{-2} K^{-4} is the Stefan Boltzman constant.

2.5.2 Cloudy sky

The clear-sky incoming radiation components from the previous section are modified for liquid water effects using an approach based on Stephens (1978). The method assumes clear and cloudy sky contributions can be treated separately.

The incoming short-wave radiation is

$$R_{sw}^{in}(\sigma) = R_{sw(clear-sky)}^{in} \Psi_{Transmission},$$

and using a fit to within 0.05 of the Ψ functions from Figure 3 of Stephens (1978) for transmission/absorption of short-wave radiation (ignoring zenith angle dependence)

$$\Psi_{Transmission} = \begin{cases} \exp\left(-16W^{in} + 13W^{in\,2}\right); & W^{in} \le 0.11 \\ 0.2; & W^{in} > 0.11 \end{cases},$$

$$\Psi_{Absorption} = \begin{cases} 0.3W^{in\,1/2}; & W^{in} \le 0.11 \\ 0.1; & W^{in} > 0.11 \end{cases}.$$

The incoming long-wave radiation is

$$R_{lw}^{in}(\sigma) = R_{lw(clear-sky)}^{in}\left(1 - \varepsilon_{lw}^{in}(\sigma)\right) + \varepsilon_{lw}^{in}(\sigma)\sigma_{SB}T^{4}(\sigma),$$
$$\varepsilon_{lw}^{in}(\sigma) = \min\left(0.9, 1 - \exp\left(-158W^{in}\right)\right),$$

with the incoming liquid water path

$$W^{in} = \int_{\sigma}^{z_T} \rho_a \min(0.0003, q_C) d\sigma.$$

Radiative heating and cooling at each model level are accounted for via the source term in the prognostic equation for temperature with

$$\left.\frac{\partial T}{\partial t}\right|_{RADIATION} = \left.\frac{\partial T}{\partial t}\right|_{RADIATION(clear-sky)} + \frac{1}{\rho c_p}\frac{\partial \Psi_{Heat}}{\partial \sigma}\frac{\partial \sigma}{\partial z},$$

where

$$\Psi_{Heat}(\sigma) = R_{sw(clear-sky)}^{in}\Psi_{Absorption} + R_{lw}^{in}(\sigma) - R_{lw}^{out}(\sigma),$$

with the incoming short-wave and long-wave components from the above expressions, and the outgoing long-wave radiation from

$$R_{lw}^{out}(\sigma) = R_{lw(clear-sky)}^{out}\left(1 - \varepsilon_{lw}^{out}(\sigma)\right) + \varepsilon_{lw}^{out}(\sigma)\sigma_{SB}T^{4}(\sigma),$$
$$\varepsilon_{lw}^{out}(\sigma) = \min\left(0.9, 1 - \exp\left(-130W^{out}\right)\right),$$

with the outgoing liquid water path $W^{out} = \int_{z_S}^{\sigma} \rho_a \min(0.0003, q_C) d\sigma$.

2.6 Surface boundary conditions

Boundary conditions for mean variables at the surface are zero velocity, π_0 from the hydrostatic equation (5), $\theta_{v0} = c_p T_0 (1 + 0.61 q_0)/\pi_0$, with $T_0 = (1-\sigma_f)T_g + \sigma_f T_f$ and $q_0 = (1-\sigma_f)q_g + \sigma_f q_f$, where σ_f is the fraction of foliage cover and subscripts g and f denote soil and foliage respectively. The soil and vegetation parameterisations described below are based on those from Kowalczyk et al. (1991).

Note that if the surface type is water, then the surface temperature is set equal to the water surface temperature, and surface moisture is set equal to the saturation value. If the surface type is permanent ice/snow, then the surface temperature is set equal to –10°C, and surface moisture is set equal to the saturation value.

2.6.1 Soil parameterisation

Equations for soil temperature T_g, moisture content η_g and specific humidity q_g are

$$\frac{\partial T_g}{\partial t} = \frac{3.72 G_g}{\rho_s c_s d_1'} - \frac{7.4(T_g - T_d)}{24 \times 3600},$$

$$\frac{\partial \eta_g}{\partial t} = -\frac{c_1\left(E_g(1-\sigma_f) - \rho_w((1-\sigma_f)P + \sigma_f P_g - R)\right)}{\rho_w d_1} - \frac{c_2(\eta_g - \eta_{eq})}{24 \times 3600},$$

$$q_g = f_{wet} q_0^* + (1 - f_{wet}) q_1,$$

where

$G_g = R_{sw}^{in}(1-\alpha_g) + R_{lw}^{in} - \sigma_{SB} T_g^4 \cos\alpha - H_g - \lambda E_g =$ soil heat flux (W m^{-2}),

$H_g = \rho c_p (\theta_g - \theta_1)/r_H =$ sensible heat flux (W m^{-2}),

$\lambda E_g = \rho\lambda(q_g - q_1)/r_H =$ evaporative heat flux (W m^{-2}),

r_H is the aerodynamic resistance (see Section 2.6.4) with a roughness length of 0.1 m,

$$\eta_{eq} = \eta_d - \eta_{sat} a_\eta \left(\frac{\eta_d}{\eta_{sat}}\right)^{b_\eta} \left(1 - \left(\frac{\eta_d}{\eta_{sat}}\right)^{8 b_\eta}\right),$$

$T_d, \eta_d =$ deep soil temperature and moisture (model input),

$\lambda = 2.5 \times 10^6$ J kg^{-1}, $\rho_w = 1000$ kg m^{-3},

$$d_1' = \sqrt{\frac{k_s \times 24 \times 3600}{\rho_s c_s \pi_c}},\ d_1 = 0.1,$$

$\alpha_g, k_s, \rho_s, c_s =$ soil albedo, conductivity, density, and heat capacity,

$P, P_g =$ precipitation reaching the vegetation and soil respectively,

$q_g^* =$ soil saturated specific humidity,

$R =$ runoff.

The soil characteristics are specified for three soil types

$$k_s = 419(a_s \eta_g - b_s \eta_g^{0.4}),$$

$$\rho_s c_s = (1-\eta_{sat})\rho_s^{dry} c_s^{dry} + \eta_g \rho_w c_w,$$

$$c_w = 4186,$$

Sand :

$$c_1 = \begin{cases} 10 & ; \text{for } \eta_r \le 0.05, \\ \dfrac{(1.8\eta_r + 0.962)}{(5.0\eta_r + 0.2)} & ; \text{otherwise.} \end{cases}$$

$$c_2 = 2.0;$$

$$f_{wet} = \begin{cases} 1 & ; \text{for } \eta_r \ge 0.15, \\ 11.49(\eta_r - 0.063) & ; \text{for } 0.063 \le \eta_r \le 0.15, \\ 0 & ; \text{for } \eta_r < 0.063. \end{cases}$$

$$\eta_r = \eta_0 / \eta_{sat}, \eta_{sat} = 0.395, \eta_{wilt} = 0.068,$$

$$a_s = 0.004, b_s = 0.006, \rho_s^{dry} = 1600, c_s^{dry} = 800, a_\eta = 0.387, b_\eta = 4.$$

Sandy Clay Loam :

$$c_1 = \begin{cases} 10 & ; \text{for } \eta_r \le 0.226, \\ \dfrac{(1.78\eta_r + 0.253)}{(2.96\eta_r - 0.581)} & ; \text{otherwise.} \end{cases}$$

$$c_2 = 3.0;$$

$$f_{wet} = \begin{cases} 1 & ; \text{for } \eta_r \ge 0.365, \\ 6.90(\eta_r - 0.22) & ; \text{for } 0.22 \le \eta_r \le 0.365, \\ 0 & ; \text{for } \eta_r < 0.22. \end{cases}$$

$$\eta_r = \eta_0 / \eta_{sat}, \eta_{sat} = 0.420, \eta_{wilt} = 0.175,$$

$$a_s = 0.003, b_s = 0.004, \rho_s^{dry} = 1600, c_s^{dry} = 845, a_\eta = 0.135, b_\eta = 6.$$

Clay :

$$c_1 = \begin{cases} 10 & ; \text{for } \eta_r \le 0.421, \\ \dfrac{(2.22\eta_r - 0.556)}{(2.78\eta_r - 1.114)} & ; \text{otherwise.} \end{cases}$$

$$c_2 = 1.9;$$

$$f_{wet} = \begin{cases} 1 & ; \text{for } \eta_r \ge 0.52, \\ 8.33(\eta_r - 0.40) & ; \text{for } 0.40 \le \eta_r \le 0.52, \\ 0 & ; \text{for } \eta_r < 0.40. \end{cases}$$

$$\eta_r = \eta_0 / \eta_{sat}, \eta_{sat} = 0.482, \eta_{wilt} = 0.286,$$

$$a_s = 0.002, b_s = 0.003, \rho_s^{dry} = 1600, c_s^{dry} = 890, a_\eta = 0.083, b_\eta = 12.$$

2.6.2 Vegetation parameterisation

The vegetation temperature T_f is calculated from a surface energy balance

$$0 = R_{sw}^{in}(1-\alpha_f) + R_{lw}^{in} - \sigma_{SB}T_f^4\cos\alpha - H_f - \lambda E_f$$

using Newton iteration, where the outward long-wave radiation and sensible (H_f) and latent (E_f) heat fluxes are treated as functions of T_f, with

$$H_f = \rho c_p(\theta_f - \theta_1)/r_H,$$
$$E_f = (1-\beta)E_{tr} + \beta E_w,$$
$$E_{tr} = \rho(q_f^* - q_1)/(r_H + r_s),$$
$$E_w = \rho(q_f^* - q_1)/r_H,$$
$$\beta = \begin{cases} 1; & \text{if condensation } (q_1 > q_f^*) \\ m_r/(0.0002LAI); & \text{if evapotranspiration} \end{cases},$$
$$\frac{\partial m_r}{\partial t} = P - P_g - \beta E_w/\rho_w,$$

where m_r is the moisture reservoir and r_H is the aerodynamic resistance (see Section 2.6.4).

The vegetation specific humidity q_f is calculated from $q_f = q_f^* - E_f r_S/\rho$, and the stomatal resistance r_S is calculated using

$$r_S = \frac{r_{si}}{LAI}F_1F_2^{-1}F_3^{-1}F_4^{-1}$$

and

$$F_1 = \frac{1+f}{f+(r_{si}/5000)},\quad F_2 = \frac{\eta_d - \eta_{wilt}}{0.75\eta_{sat} - \eta_{wilt}},$$

$$F_3 = 1 - 0.00025(e_f^* - e_1),\quad F_4 = 1 - 0.0016(298 - T_1)^2,\quad f = 0.55\frac{\mathrm{R}_{\mathrm{sw}}^{\mathrm{in}}}{\mathrm{R}^*}\frac{2}{LAI}.$$

Other variables are

α_f = Vegetation albedo (0.2),

q_f^* = Vegetation saturated specific humidity,

e_f^* = Vegetation saturated vapour pressure,

$$R^* = \begin{cases} 30\ \mathrm{W\ m^{-2}}; & \text{if } z_{0f} > 0.3 \\ 100\ \mathrm{W\ m^{-2}}; & \text{if } z_{0f} \le 0.3 \end{cases},$$

z_{0f} = vegetation roughness length (m) $= 0.1 + h_f/10$ $(z_{0f} \le 2.0\ \mathrm{m})$,

h_f = vegetation height (m),

σ_f = fraction of surface covered by vegetation,

LAI = Leaf Area Index,

r_{si} = minimum stomatal resistance (s^{-1}).

Table 1: Vegetation (land-use) characteristics used in TAPM.

Vegetation Types:	h_f (m)	σ_f	LAI	r_{si} (m^{-1})
-1: Permanent snow/ice	-	-	-	-
0: Water	-	-	-	-
1: Forest – tall dense	42.00	0.75	4.8	370
2: Forest – tall mid-dense	36.50	0.75	6.3	330
3: Forest – dense	25.00	0.75	5.0	260
4: Forest – mid-dense	17.00	0.50	3.8	200
5: Forest – sparse (woodland)	12.00	0.25	2.8	150
6: Forest – very sparse (woodland)	10.00	0.25	2.5	130
7: Forest – low dense	9.00	0.75	3.9	200
8: Forest – low mid-dense	7.00	0.50	2.8	150
9: Forest – low sparse (woodland)	5.50	0.25	2.0	110
10: Shrub-land – tall mid-dense (scrub)	3.00	0.50	2.6	160
11: Shrub-land – tall sparse	2.50	0.25	1.7	100
12: Shrub-land – tall very sparse	2.00	0.25	1.9	120
13: Shrub-land – low mid-dense	1.00	0.50	1.4	90
14: Shrub-land – low sparse	0.60	0.25	1.5	90
15: Shrub-land – low very sparse	0.50	0.25	1.2	80
16: Grassland – sparse hummock	0.50	0.25	1.6	90
17: Grassland – very sparse hummock	0.45	0.25	1.4	90
18: Grassland – dense tussock	0.75	0.75	2.3	150
19: Grassland – mid-dense tussock	0.60	0.50	1.2	80
20: Grassland – sparse tussock	0.45	0.25	1.7	100
21: Grassland – very sparse tussock	0.40	0.25	1.2	80
22: Pasture/herb-field – dense (perennial)	0.60	0.75	2.3	80
23: Pasture/herb-field – dense (seasonal)	0.60	0.75	2.3	80
24: Pasture/herb-field – mid-dense (perennial)	0.45	0.50	1.2	40
25: Pasture/herb-field – mid-dense (seasonal)	0.45	0.50	1.2	40
26: Pasture/herb-field – sparse	0.35	0.25	1.9	120
27: Pasture/herb-field – very sparse	0.30	0.25	1.0	80
28: Littoral	2.50	0.50	3.0	180
29: Permanent lake	-	-	-	-
30: Ephemeral lake (salt)	-	-	-	-
31: Urban	10.00	0.75	2.0	100
32: Urban (low)	8.00	0.75	2.0	100
33: Urban (medium)	12.00	0.75	2.0	100
34: Urban (high)	16.00	0.75	2.0	100
35: Urban (cbd)	20.00	0.75	2.0	100
36: Industrial (low)	10.00	0.75	2.0	100
37: Industrial (medium)	10.00	0.75	2.0	100
38: Industrial (high)	10.00	0.75	2.0	100

The vegetation (land-use) types used in TAPM are based on a CSIRO Wildlife and Ecology Categorisation (Graetz, 1998, personal communication), and are listed in Table 1, with urban/industrial conditions modified as described in Section 2.6.3.

2.6.3 Urban Parameterisation

The generic urban land-use category (31) contained in the default databases can be thought of as medium density urban conditions, with parameters specified in Table 2 based on Oke (1988) and Pielke (1984). Other urban/industrial land-use categories listed in Table 2, not currently in the default databases, can also be selected through the model user interface (parameters for categories 32-35 are from McDonald Coutts, 2004, personal communication).

In urban regions the surface temperature and specific humidity are calculated using $T_0 = (1-\sigma_U)T_{g\&f} + \sigma_U T_U$ and $q_0 = (1-\sigma_U)q_{g\&f} + \sigma_U q_U$, where σ_U is the fraction of urban cover, and subscript *U* denotes urban and *g*&*f* denotes the combined soil and foliage values respectively.

The equations for urban temperature T_U and specific humidity q_U use a similar approach as that for soil temperature, except that the surface properties are those of urban surfaces such as concrete/asphalt/roofs/etc:

$$\frac{\partial T_U}{\partial t} = \frac{3.72 G_U}{\rho_U c_U d_U} - \frac{7.4(T_U - T_d)}{24 \times 3600},$$

$$q_U = 0,$$

where

$$G_U = R_{sw}^{in}(1-\alpha_U) + R_{lw}^{in} - \varepsilon_U \sigma_{SB} T_U^4 \cos\alpha - H_U - \lambda E_U + A_U$$

$$= \text{urban surface heat flux (W m}^{-2}),$$

$$H_U = \rho c_p (\theta_U - \theta_1)/r_H = \text{urban sensible heat flux (W m}^{-2}),$$

$$\lambda E_U = 0 = \text{urban evaporative heat flux (W m}^{-2}),$$

$$d_U = \sqrt{\frac{k_U \times 24 \times 3600}{\rho_U c_U \pi_c}},$$

A_U = urban anthropogenic heat flux (W m^{-2}),

$\varepsilon_U = 0.95$ = urban emissivity,

$\rho_U = 2300$ kg m^{-3} = urban density,

$c_U = 879$ J kg^{-1} K^{-1} = urban heat capacity,

α_U, k_U = urban albedo and conductivity.

Note that the anthropogenic heat flux (A_U) is also included in the soil and vegetation surface flux equations when the land-use category is urban/industrial.

Urban surface layer scaling variables are calculated using the same approach as for soil and vegetation, incorporating the corresponding urban roughness length (z_{oU}).

Table 2: Urban/Industrial land-use characteristics used in TAPM.

Land-use Types:	σ_U	α_U	A_U	k_U	z_{oU}
31: Urban	0.50	0.15	30	4.6	1.0
32: Urban (low)	0.50	0.17	20	1.5	0.4
33: Urban (medium)	0.65	0.15	30	5.0	0.6
34: Urban (high)	0.80	0.13	40	8.0	0.8
35: Urban (cbd)	0.95	0.10	70	10.0	2.0
36: Industrial (low)	0.50	0.15	50	4.6	0.5
37: Industrial (medium)	0.65	0.15	100	4.6	1.0
38: Industrial (high)	0.80	0.15	150	4.6	1.5

2.6.4 Surface fluxes and turbulence

Boundary conditions for the turbulent fluxes are determined by Monin-Obukhov surface layer scaling variables with stability functions from Dyer and Hicks (1970)

$$\overline{w'u'}\big|_0 = -u_*^2 u\Big/\sqrt{u_1^2+v_1^2}\,,\ \ \overline{w'v'}\big|_0 = -u_*^2 v\Big/\sqrt{u_1^2+v_1^2}\,,\ \ \overline{w'\theta_v'}\big|_0 = -u_*\theta_{v*},\ \ \overline{w'q'}\big|_0 = -u_* q_*.$$

where

$$u_* = k\sqrt{u_1^2+v_1^2}\,/\,I_M\,,\ \theta_{v*} = k(\theta_{v1}-\theta_{v0})/I_H\,,\ \theta_* = k(\theta_1-\theta_0)/I_H\,,\ q_* = k(q_1-q_0)/I_H\,,$$

$$I_M = \begin{cases} \ln\left(\dfrac{z_1}{z_0}\right) - 2\ln\left(\dfrac{1+\phi_M^{-1}(z_1)}{1+\phi_M^{-1}(z_0)}\right) - \ln\left(\dfrac{1+\phi_M^{-2}(z_1)}{1+\phi_M^{-2}(z_0)}\right) \\ \qquad + 2\left(\tan^{-1}\left(\phi_M^{-1}(z_1)\right) - \tan^{-1}\left(\phi_M^{-1}(z_0)\right)\right), \text{ if } \dfrac{z_1}{L} < 0, \\ \ln\left(\dfrac{z_1}{z_0}\right) + 5\left(\dfrac{z_1-z_0}{L}\right), \text{if } \dfrac{z_1}{L} \ge 0 \end{cases}$$

$$I_H = I_{aH} + I_{bH},$$

$$I_{aH} = \begin{cases} \ln\left(\dfrac{z_1}{z_0}\right) - 2\ln\left(\dfrac{1+\phi_H^{-1}(z_1)}{1+\phi_H^{-1}(z_T)}\right), \text{if } \dfrac{z_1}{L} < 0 \\ \ln\left(\dfrac{z_1}{z_0}\right) + 5\left(\dfrac{z_1-z_T}{L}\right), \text{if } \dfrac{z_1}{L} \ge 0 \end{cases},$$

$$I_{bH} = \ln\left(\frac{z_0}{z_T}\right),$$

$$r_H = I_H/(ku_*),\ r_{aH} = I_{aH}/(ku_*),\ r_{bH} = I_{bH}/(ku_*),$$

$$\phi_M = \begin{cases} \left(1-16\dfrac{z}{L}\right)^{-1/4}; \text{for } \dfrac{z}{L} < 0 \\ \left(1+5\dfrac{z}{L}\right); \quad \text{for } \dfrac{z}{L} \ge 0 \end{cases},\ \phi_H = \begin{cases} \left(1-16\dfrac{z}{L}\right)^{-1/2}; \text{for } \dfrac{z}{L} < 0 \\ \left(1+5\dfrac{z}{L}\right); \quad \text{for } \dfrac{z}{L} \ge 0 \end{cases},$$

with $\frac{z}{L} = \frac{kzg\theta_{v*}}{u_*^2\theta_v}$, and $z_T = z_0/7.4$ from Garratt (1992),

and the gradient Richardson number $R_{ig} = \frac{z}{L}\frac{\phi_H}{\phi_M^2}$,

which in the stable limit gives a critical value of $R_{igc} = 0.2$.

These equations are solved iteratively, with the restrictions that $z_1 / L \le 1$ and $0.01 \le u_* \le 2.0$ m s^{-1}.

Turbulence boundary conditions are specified at the first model level using surface and mixed layer scaling, for the prognostic turbulence equations

$$E = c_m^{-1/2}u_*^2 + 0.5w_*^2 \text{ and } \varepsilon = \frac{u_*^3}{kz}\phi_m - \frac{g}{\theta_v}u_*\theta_{v*},$$

where w_* is the convective velocity scale (m s^{-1}) defined as

$$w_* = \left(\frac{-gz_i u_*\theta_{v*}}{\theta_v}\right)^{1/3},$$

and z_i is the convective boundary-layer height (m). The boundary-layer height in convective conditions is defined as the first model level above the surface for which the vertical heat flux is negative, while in stable/neutral conditions it is defined as the first model level above the surface that has a vertical heat flux less than 5% of the surface value following Derbyshire (1990).

2.7 Initial conditions and boundary conditions

The model is initialised at each grid point with values of $u_s, v_s, \theta_{vs}, q_s$ interpolated from the synoptic analyses. Iso-lines of these variables are oriented to be parallel to mean sea level (i.e. cutting into the terrain). Turbulence levels are set to their minimum values as the model is started at midnight. The Exner pressure function is integrated from mean sea level to the model top to determine the top boundary condition. The Exner pressure and terrain-following vertical velocity are then diagnosed using equations (3) and (5) respectively. Surface temperature and moisture are set to the deep soil values specified, with surface temperature adjusted for terrain height using the synoptic lapse rate. At the model top boundary, all variables are set at their synoptic values.

One-way nested lateral boundary conditions are used for the prognostic equations (1), (2), (4), and (7) using an approach based on Davies (1976). For example for *u*, an additional term is added to the right hand side of equation (1).

$$\frac{du}{dt} = RHS(u) - F_{NEST}\frac{(u - \tilde{u})}{3\Delta t}$$

where $\tilde{u}$ is interpolated from the coarse outer grid onto the fine inner grid, and

$$F_{NEST} = \max(G_x, G_y)$$

$$G_x = \begin{cases} 1-\left(\dfrac{i-1}{n_b}\right)^2; & \text{for } i = 1,...,n_b; \\ 1-\left(\dfrac{n_x - i}{n_b}\right)^2; & \text{for } i = n_x-(n_b-1),...,n_x; \\ 0; & \text{otherwise.} \end{cases}$$

and similarly for G_y, with n_x the number of grid points in the *x* direction, and $n_b = 5$ the number of grid points in from the grid edge over which the solutions are meshed. On the outer grid, this same nesting procedure is used, but using time-interpolated synoptic winds, temperature and moisture. Note that the terrain is smoothed near the lateral boundaries to reduce noise created by the boundary conditions.

2.8 Assimilation of wind observations

The method used to optionally assimilate wind observations is based on the approach of Stauffer and Seaman (1994), where a nudging term is added to the horizontal momentum equations (for *u* and *v*). The equation for *u* is

$$\frac{\partial u}{\partial t} = RHS(u) + G\left(\frac{\sum_{n=1}^{nsite} W_n\left(u_n - \hat{u}_n\right)}{\sum_{n=1}^{nsite} W_n}\right),$$

where

G = nudging coefficient $= 1/(3\Delta t)$,

Δt = model meteorological advection timestep,

u_n = observed u at observation site n,

$\hat{u}_n$ = model u interpolated to observation site n,

$$W_n = \begin{cases} Q_n\left(\dfrac{R_n^2 - D_n^2}{R_n^2 + D_n^2}\right); & \text{if } D_n < R_n; \\ 0; & \text{otherwise.} \end{cases}$$

Q_n = data quality indicator [0...1],

R_n = radius of influence (m),

$D_n^2 = (x_i - x_n)^2 + (y_j - y_n)^2$,

(x_i, y_j) = location of grid point,

(x_n, y_n) = location of observation site.

Note that observations at any height can be included, and the observations can influence a user-specified number of model levels for each site.

3 Air pollution component

3.1 Eulerian grid module

The Eulerian Grid Module (EGM) consists of nested grid-based solutions of the Eulerian concentration mean and optionally variance equations representing advection, diffusion, chemical reactions and emissions. Dry and wet deposition processes are also included.

3.1.1 Pollutant equations

3.1.1.1 Mean Concentration

The prognostic equation for concentration χ is similar to that for the potential virtual temperature and specific humidity variables, and includes advection, diffusion, and terms to represent pollutant emissions S_χ and chemical reactions R_χ

$$\frac{d\chi}{dt} = \frac{\partial}{\partial x}\left(K_{H\chi}\frac{\partial \chi}{\partial x}\right) + \frac{\partial}{\partial y}\left(K_{H\chi}\frac{\partial \chi}{\partial y}\right) - \left(\frac{\partial \sigma}{\partial z}\right)\frac{\partial}{\partial \sigma}\left(\overline{w'\chi'}\right) + S_\chi + R_\chi . \tag{11}$$

The vertical flux of concentration includes counter-gradient fluxes as follows

$$\overline{w'\chi'} = -K_\chi \frac{\partial \chi}{\partial \sigma}\frac{\partial \sigma}{\partial z} + \frac{(1-c_{\chi 3})}{c_{\chi 1}}\frac{E}{\varepsilon}\frac{g}{\theta_v}\overline{\theta_v'\chi'}$$

with

$$\begin{aligned}\frac{d\overline{\theta_v'\chi'}}{dt} = {} & \frac{\partial}{\partial x}\left(K_{H\chi}\frac{\partial \overline{\theta_v'\chi'}}{\partial x}\right) + \frac{\partial}{\partial y}\left(K_{H\chi}\frac{\partial \overline{\theta_v'\chi'}}{\partial y}\right) + \left(\frac{\partial \sigma}{\partial z}\right)^2 \frac{\partial}{\partial \sigma}\left(K_\chi \frac{\partial \overline{\theta_v'\chi'}}{\partial \sigma}\right) \\ & + \left(K + K_\chi\right)\left(\left(\frac{\partial \theta_v}{\partial x} + \frac{\partial \theta_v}{\partial \sigma}\frac{\partial \sigma}{\partial x}\right)\left(\frac{\partial \chi}{\partial x} + \frac{\partial \chi}{\partial \sigma}\frac{\partial \sigma}{\partial x}\right) + \left(\frac{\partial \theta_v}{\partial y} + \frac{\partial \theta_v}{\partial \sigma}\frac{\partial \sigma}{\partial y}\right)\left(\frac{\partial \chi}{\partial y} + \frac{\partial \chi}{\partial \sigma}\frac{\partial \sigma}{\partial y}\right)\right) \\ & - \overline{w'\theta_v'}\frac{\partial \chi}{\partial \sigma}\frac{\partial \sigma}{\partial z} - \overline{w'\chi'}\frac{\partial \theta_v}{\partial \sigma}\frac{\partial \sigma}{\partial z} - \frac{2}{c_\chi}\frac{\varepsilon}{E}\overline{\theta_v'\chi'}.\end{aligned} \tag{12}$$

Constants in these equations are $c_{\chi 1} = 3.0$, $c_{\chi 3} = 0.5$, and $c_\chi = 1.6$, based on those used by Rodi (1985). The form of these equations has been used in many of the second order closure models for a meteorological scalar, and has been used by Enger (1986) for dispersion in a convective boundary layer, although he also used a prognostic equation for $\overline{w'\chi'}$. The diffusion coefficients used for pollutant concentration are $K_{H\chi} = \min\left(10, K_\chi\right)$ and $K_\chi = 2.5K$, consistent with meteorological variables (see Section 2.4).

Initially χ is set to a background concentration. Values of $\overline{\theta_v'\chi'}$ are initialised to zero as conditions are thermally stable, and if counter-gradient fluxes are assumed unimportant for a particular simulation, the solution of equation (12) is omitted and $\overline{\theta_v'\chi'}$ is set to zero. For concentration at inflow boundaries on the outermost grid, a background concentration is specified, while values at the boundaries of inner grids are obtained from the previous nest. At outflow boundaries, zero gradient boundary conditions are used. Zero gradient boundary conditions are used for $\overline{\theta_v'\chi'}$ on all grids.

3.1.1.2 Concentration Variance and Peak-to-Mean Concentration

In tracer mode, or for SO_2 in chemistry mode, concentration variance $\overline{\chi'^2}$ can be computed using the following prognostic equation:

$$\frac{d\overline{\chi'^2}}{dt} = \frac{\partial}{\partial x}\left(K_{H\chi}\frac{\partial\overline{\chi'^2}}{\partial x}\right) + \frac{\partial}{\partial y}\left(K_{H\chi}\frac{\partial\overline{\chi'^2}}{\partial y}\right) + \left(\frac{\partial\sigma}{\partial z}\right)^2\frac{\partial}{\partial\sigma}\left(K_{\chi}\frac{\partial\overline{\chi'^2}}{\partial\sigma}\right) + P_V - \varepsilon_V + S_V,$$

with production term:

$$P_V = \begin{cases} 2K_{\chi}\left(\left(\frac{\partial\overline{\chi}}{\partial x} + \frac{\partial\overline{\chi}}{\partial\sigma}\frac{\partial\sigma}{\partial x}\right)^2 + \left(\frac{\partial\overline{\chi}}{\partial y} + \frac{\partial\overline{\chi}}{\partial\sigma}\frac{\partial\sigma}{\partial y}\right)^2 + \left(\frac{\partial\overline{\chi}}{\partial\sigma}\frac{\partial\sigma}{\partial z}\right)^2\right), & \text{if } \overline{\chi} \text{ in EGM mode;} \\ 2c_{k(LPM)}K\left(\left(\frac{\partial\overline{\chi}}{\partial x} + \frac{\partial\overline{\chi}}{\partial\sigma}\frac{\partial\sigma}{\partial x}\right)^2 + \left(\frac{\partial\overline{\chi}}{\partial y} + \frac{\partial\overline{\chi}}{\partial\sigma}\frac{\partial\sigma}{\partial y}\right)^2 + \left(\frac{\partial\overline{\chi}}{\partial\sigma}\frac{\partial\sigma}{\partial z}\right)^2\right), & \text{if } \overline{\chi} \text{ in LPM mode;} \end{cases},$$

concentration variance dissipation rate:

$$\varepsilon_{\chi} = \frac{2}{c_{\chi}}\frac{\varepsilon}{E}\overline{\chi'^2},$$

and the emission source term

$$S_V = 2I_E\left(\overline{\chi'^2}\right)^{1/2}S_{\chi},$$

with the emission concentration fluctuation intensity set to $I_E = 0.5$ for all sources.

The constants c_k and c_{χ} are the same as for the concentration and potential virtual temperature cross-correlation prognostic equation. Note that $c_{k(LPM)} = 0.3$ represents the scalar diffusivity coefficient when LPM mean concentration is used. Ideally, concentration variance should be calculated using a Lagrangian approach when in LPM mode, but nevertheless, results from the current approach give good near-source concentration variance for point sources in LPM mode. The concentration variance $\overline{\chi'^2}$ is initially set to zero and uses zero gradient boundary conditions on all grids.

The calculation of peak-to-mean concentration is performed when pollution is post-processed. The maximum hourly-averaged concentration is enhanced to obtain peak concentration estimates for 10-minute, 3-minute, 1-minute and 1-second averaging periods. Peak concentrations are calculated using the commonly used power-law relationship, but with an exponent that depends on concentration fluctuation intensity I_C (derived from the mean and variance of the concentration output from the model)

$$C_{MAX}(t) = C_{MAX}(3600)\left(\frac{3600}{t}\right)^{\min\left(0.1+0.25I_C^{1/3},0.4\right)},$$

with *t* the averaging period (s), and

$$I_C = \left(\frac{\overline{\chi'^2}}{\overline{\chi}^2}\right)^{1/2}.$$

Note that the peak-to-mean approach is only valid for long time-series, and is typically used for results from annual model runs.

3.1.2 Chemistry and Aerosols

The model can be run in either tracer mode, chemistry mode, or dust mode. In tracer mode, the only chemical reaction is an optional exponential decay $R_\chi = -k_{decay}\chi$, where the decay rate k_{decay} is a model input. In chemistry mode, gas-phase photochemistry is based on the semi-empirical mechanism called the Generic Reaction Set (GRS) of Azzi et al. (1992), with the hydrogen peroxide modification of Venkatram et al. (1997). We have also included gas- and aqueous-phase reactions of sulfur dioxide and particles, with the aqueous-phase reactions based on Seinfeld and Pandis (1998). In dust mode, pollutant concentration is calculated for four particle size ranges: $PM_{2.5}$, PM_{10}, PM_{20} and PM_{30}. The emissions, background concentrations and output concentrations are relevant for these four categories, while calculations in the model are actually done for $PM_{2.5}$, PM_{10}, $PM_{10\text{-}20}$ and $PM_{20\text{-}30}$. This categorisation allows representative particle sizes to be used to account for particle settling and dry/wet deposition. Exponential decay of particles is also allowed, as is available in tracer mode, but there are no chemical transformations or particle growth processes included.

In chemistry mode, there are ten reactions for thirteen species: smog reactivity (R_{smog}), the radical pool (RP), hydrogen peroxide (H_2O_2), nitric oxide (NO), nitrogen dioxide (NO_2), ozone (O_3), sulfur dioxide (SO_2), stable non-gaseous organic carbon (SNGOC), stable gaseous nitrogen products (SGN), stable non-gaseous nitrogen products (SNGN), stable non-gaseous sulfur products (SNGS), plus Airborne Particulate Matter (APM) and Fine Particulate Matter (FPM) that include secondary particulate concentrations consisting of (SNGOC), (SNGN), and (SNGS).

The reactions are

Reactions	*Reaction Rates*
$R_{smog} + h\nu \rightarrow RP + R_{smog} + \eta SNGOC$	$R_1 = k_1[R_{smog}]$
$RP + NO \rightarrow NO_2$	$R_2 = k_2[RP][NO]$
$NO_2 + h\nu \rightarrow NO + O_3$	$R_3 = k_3[NO_2]$
$NO + O_3 \rightarrow NO_2$	$R_4 = k_4[NO][O_3]$
$RP + RP \rightarrow RP + \alpha H_2O_2$	$R_5 = k_5[RP][RP]$
$RP + NO_2 \rightarrow SGN$	$R_6 = k_6[RP][NO_2]$
$RP + NO_2 \rightarrow SNGN$	$R_7 = k_7[RP][NO_2]$
$RP + SO_2 \rightarrow SNGS$	$R_8 = k_8[RP][SO_2]$
$H_2O_2 + SO_2 \rightarrow SNGS$	$R_9 = k_9[H_2O_2][SO_2]$
$O_3 + SO_2 \rightarrow SNGS$	$R_{10} = k_{10}[O_3][SO_2]$

where [*A*] denotes concentration of species *A* and *hν* denotes photo-synthetically active radiation.

Yield coefficients are

$$\alpha = \max\left(0.03, \exp\left(-0.0261\frac{[R_{smog}]}{[NO_X]}\right)\right),$$

$$\eta = 0.1,$$

and reaction rate coefficients are

$$k_1 = k_3 f,$$
$$k_2 = 3580/(60T),$$
$$k_3 = 0.0001\delta.TSR/60,$$
$$k_4 = (924/60T)\exp(-1450/T),$$
$$k_5 = (10/60),$$
$$k_6 = (0.12/60),$$
$$k_7 = k_6,$$
$$k_8 = (0.003/60),$$
$$k_9 = \frac{7.45\times10^7[H^+]\alpha_1}{1+13[H^+]}K_{H\_S(IV)}K_{H\_H_2O_2}L\cdot R\cdot T\cdot10^{-9},$$
$$k_{10} = (2.4\times10^4\alpha_0 + 3.7\times10^5\alpha_1 + 1.5\times10^9\alpha_2)K_{H\_S(IV)}K_{H\_O_3}L\cdot R\cdot T\cdot10^{-9},$$

with

$$[H^+] = 10^{-pH},$$
$$\alpha_0 = \frac{K_{H0\_SO_2}}{K_{H\_S(IV)}}, \alpha_1 = \alpha_0\frac{K_{H1\_SO_2}}{[H^+]}, \alpha_2 = \alpha_1\frac{K_{H2\_SO_2}}{[H^+]},$$
$$K_{H\_S(IV)} = K_{H0\_SO_2}\left(1+\frac{K_{H1\_SO_2}}{[H^+]}\left(1+\frac{K_{H2\_SO_2}}{[H^+]}\right)\right),$$
$$K_{H0\_SO_2} = 1.24\exp\left(-3120\left(\frac{1}{298}-\frac{1}{T}\right)\right),$$
$$K_{H1\_SO_2} = 1.29\times10^{-2}\exp\left(-2080\left(\frac{1}{298}-\frac{1}{T}\right)\right),$$
$$K_{H2\_SO_2} = 6.014\times10^{-8}\exp\left(-1120\left(\frac{1}{298}-\frac{1}{T}\right)\right),$$
$$K_{H\_H_2O_2} = 7.1\times10^4\exp\left(-7250\left(\frac{1}{298}-\frac{1}{T}\right)\right),$$
$$K_{H\_O_3} = 9.4\times10^{-3}\exp\left(-2520\left(\frac{1}{298}-\frac{1}{T}\right)\right),$$
$$(\text{all } K_H \le (L\cdot R\cdot T)^{-1}),$$

where APM and FPM are in µg m^{-3}, all other species are in units of ppb, the rate coefficients k_1, k_3 are in s^{-1} and $k_2, k_4, k_5, k_6, k_7, k_8, k_9, k_{10}$ are in ppb^{-1} s^{-1}, temperature *T* is in K, the total

solar radiation *TSR* is in W m^{-2}, *R* is the gas constant (0.082) in atm M^{-1} K^{-1}, *L* is the volume based liquid water fraction related to the liquid water specific humidity by $L = q_L \rho / \rho_W$,

$$f = \exp\left(-4700\left(\frac{1}{T} - \frac{1}{316}\right)\right),$$

$$\delta = \begin{cases} 4.23 + 1.09 / \cos Z; & \text{if } 0 \le Z \le 47 \\ 5.82; & \text{if } 47 \le Z \le 64 \\ -0.997 + 12(1 - \cos Z); & \text{if } 64 \le Z \le 90 \end{cases},$$

and *Z* is the zenith angle in degrees.

The yield factor η, the reaction rate k_8, and the secondary formation of APM and FPM by the various processes, are in a preliminary form that needs to be verified against appropriate data.

The concept of using R_{smog} rather than Volatile Organic Compounds (VOCs) in the reaction equations follows from the work of Johnson (1984). The concentration of R_{smog} is defined as a reactivity coefficient multiplied by VOC concentration. For example, Johnson (1984) used $[R_{smog}] = 0.0067[VOC]$ for typical 1980s Australian urban air dominated by motor vehicles. Empirically determined reactivity coefficients for individual VOC species are available from smog chamber experiments, while numerically determined reactivity coefficients have been calculated by comparison of the GRS mechanism with more complex mechanisms (Cope, 1999, personal communication).

Table 3 : Characteristics of the CBIV lumped VOC species needed for the GRS mechanism (Cope, 1999, personal communication).

CBIV Lumped VOC Species (*i*)	Carbon Number (CN_i)	Molecular Weight (MW_i)	CBIV Reactivity (a_i) (ppb ppbC^{-1}) (URBAN)
Formaldehyde (FORM) (CH_20)	1	30	0.0174
Higher Aldehydes (ALD2) (C_2H_40)	2	44	-0.00081
Ethene (ETH) (C_2H_4)	2	28	0.0153
Alkenes (Olefins) (OLE) (C_2H_4)	2	28	0.0127
Alkanes (Paraffins) (PAR) (CH_2)	1	14	0.00095
Toluene (TOL) (C_7H_8)	7	92	0.0049
Xylene (XYL) (C_8H_{10})	8	106	0.0145
Isoprene (ISOP) (C_5H_8)	5	68	0.0092

Emissions from VOC sources usually consist of more than one type of VOC, necessitating the R_{smog} emission rate to be calculated in the following way

$$Q_{Rsmog} = \sum_i \frac{14 CN_i}{MW_i} a_i Q_i ,$$

where Q_i is the emission rate (g s^{-1}) for each VOC, a_i is its reactivity, CN_i is its carbon number and MW_i is its molecular weight. An alternative (and more precise) approach is to use a

standard reactivity coefficient for a standard VOC mixture (for example $Q_{Rsmog} = 0.0067 Q_{VOC}$) with perturbations about this standard accounted for using the individual species reactivity coefficients (M. Cope, 1999, personal communication). Sample perturbation coefficients for the Carbon Bond IV (CBIV) and the updated Carbon Bond IV (CBIV_99) mechanisms are summarised in Tables 3 and 4 respectively. More detail on the perturbation coefficients summarised in Table 4 are given in Hurley et al., (2003).

Table 4 : Characteristics of the CBIV_99 lumped VOC species needed for the GRS mechanism (Cope, 2003, personal communication).

CBIV Lumped VOC Species (*i*)	Carbon Number (CN_i)	Molecular Weight (MW_i)	CBIV_99 Reactivity (a_i) (ppb ppbC^{-1}) (URBAN)	CBIV_99 Reactivity (a_i) (ppb ppbC^{-1}) (RURAL)
Formaldehyde (FORM) (CH_20)	1	30	0.0350	0.0350
Higher Aldehydes (ALD2) (C_2H_40)	2	44	0.0100	0.0150
Ethene (ETH) (C_2H_4)	2	28	0.0070	0.0140
Alkenes (Olefins) (OLE) (C_2H_4)	2	28	0.0080	0.0180
Alkanes (Paraffins) (PAR) (CH_2)	1	14	0.0000	0.0005
Toluene (TOL) (C_7H_8)	7	92	0.0008	0.0016
Xylene (XYL) (C_8H_{10})	8	106	0.0080	0.0140
Isoprene (ISOP) (C_5H_8)	5	68	0.0090	0.0300

If we define $[NO_X] = [NO] + [NO_2]$ and $[SP_X] = [O_3] + [NO_2]$ (analogous to the definition of smog produced by Johnson, 1984, but without including SGN and SNGN), we do not need the differential equations for NO and O_3. The resulting reaction terms for the prognostic equation (11) for the nine pollutants APM, FPM, SO_2, NO_X, R_{smog}, SP_X, NO_2, RP, and H_2O_2 are

$$R_{[APM]} = F_{CH2}\eta R_1 + F_{HNO3} R_7 + F_{H2SO4}\left(R_8 + R_9 + R_{10}\right)$$

$$R_{[FPM]} = F_{CH2}\eta R_1 + 0.5 F_{HNO3} R_7 + F_{H2SO4}\left(R_8 + R_9 + R_{10}\right)$$

$$R_{[SO_2]} = -R_8 - R_9 - R_{10}$$

$$R_{[NO_X]} = -R_6 - R_7$$

$$R_{[R_{smog}]} = 0$$

$$R_{[SP_X]} = R_2 - R_6 - R_7 - R_{10}$$

$$R_{[NO_2]} = R_2 - R_3 + R_4 - R_6 - R_7$$

$$R_{[RP]} = R_1 - R_2 - R_5 - R_6 - R_7 - R_8$$

$$R_{[H_2O_2]} = \alpha R_5 - R_9$$

where $F_{HNO3} = 2.6, F_{H2SO4} = 4.0, F_{CH2} = 0.57$, are approximate factors to convert the stable non-gaseous compounds to APM in µg m^{-3} at NTP.

The potentially fast reactions in the reduced system are for SO_2, NO_2, RP, and H_2O_2. This implies that a small explicit timestep is necessary, but this restriction can be overcome by

using a simple implicit solution procedure described later. This approach then allows large numerical time-steps to be used, provided the pH of the liquid water present is below about 5.5 (so that the reaction between O_3 and SO_2 to produce SNGS (R_{10}) does not dominate the aqueous phase reactions). Note that the default pH of the liquid water present in the model is 4.5, which is typical of Australian conditions.

3.1.3 Deposition and Particle Settling

The dry deposition formulation for gaseous pollutants follows that of Physick (1994) in which all scalars behave like heat in terms of roughness length and stability function. Knowing the resistance functions for heat transfer r_{aH} and r_{bH} (Section 2.6.4), and the stomatal resistance r_S (Section 2.6.2), the surface flux for variable χ is written as $\overline{w'\chi'}\big|_o = -\chi_1 V_d$, where the pollutant deposition velocity is $V_d = \left(r_{aero} + r_{surface}\right)^{-1}$, the aerodynamic resistance is $r_{aero} = r_{aH} + r_{bH} Sc^{2/3}$, the surface resistance $r_{surface}$ depends on the surface type, and Sc is the Schmidt Number (the ratio of the molecular diffusivities for water vapour and pollutant concentration).

For a land surface, $V_d = \dfrac{\sigma_f \beta}{r_{aero} + r_{water}} + \dfrac{\sigma_f (1-\beta)}{r_{aero} + r_S Sc} + \dfrac{(1-\sigma_f)}{r_{aero} + r_{soil}}$

and for a water surface, $V_d = \dfrac{1}{r_{aero} + r_{water}}$.

Non-zero deposition velocities are used for the gaseous pollutants NO_2, NO, O_3, SO_2 and H_2O_2, with resistance values based on information in Wesley (1989) and Harley et al. (1993)

NO_2: $r_{water} = 1500, r_{soil} = 500, Sc = \sqrt{46/18}$,

NO: $r_{water} = 10000, r_{soil} = 10000, Sc = \sqrt{30/18}$;

O_3: $r_{water} = 2000, r_{soil} = 400, Sc = \sqrt{48/18}$;

SO_2: $r_{water} = 0, r_{soil} = 1000, Sc = \sqrt{64/18}$;

H_2O_2: $r_{water} = 0, r_{soil} = 100, Sc = \sqrt{34/18}$.

The method for calculating the dry deposition velocity for aerosols is based on the approach of Seinfeld and Pandis (1998). The deposition velocity is calculated using $V_d = \dfrac{1}{r_{aH} + r_{bH} + r_{aH} r_{bH} V_S} + V_S$, where the resistance functions for heat transfer r_{aH} and r_{bH} and the particle settling velocity V_S are known, and the surface (water, soil, stomatal) resistance is assumed to be zero.

The quasi-laminar resistance r_{bH} accounts for Schmidt number (*Sc*) and Stokes number (*St*) dependence as follows:

$$r_{bH} = \frac{1}{u_* \left(Sc^{-2/3} + 10^{-3/St}\right)}$$

with

$Sc = \nu / D,$

$\nu = 1.58 \times 10^{-5}\ \mathrm{m^2\ s^{-1}},$

$$D = \text{diffusivity of species} = \begin{cases} 1.00\times10^{-12}\ \text{m}^2\ \text{s}^{-1} \text{ for } \text{PM}_{20\text{-}30}, \\ 1.90\times10^{-12}\ \text{m}^2\ \text{s}^{-1} \text{ for } \text{PM}_{10\text{-}20}, \\ 6.10\times10^{-12}\ \text{m}^2\ \text{s}^{-1} \text{ for } \text{PM}_{10} \text{ or APM}, \\ 2.74\times10^{-11}\ \text{m}^2\ \text{s}^{-1} \text{ for } \text{PM}_{2.5} \text{ or FPM}, \end{cases}$$

and

$$St = \frac{V_S u_*^2}{g\nu},$$

$$V_S = \frac{gC_C\rho_P D_P^2}{18\mu},$$

with

$$g = 9.81\,\text{m s}^{-2},\ \rho_P = 1000\,\text{kg m}^{-3},\ \mu = 1.8\times10^{-5}\ \text{kg m}^{-1}\ \text{s}^{-1},$$

$$C_C = \begin{cases} 1.01 \text{ for } \text{PM}_{20\text{-}30}, \\ 1.01 \text{ for } \text{PM}_{10\text{-}20}, \\ 1.05 \text{ for } \text{PM}_{10} \text{ or APM}, \\ 1.16 \text{ for } \text{PM}_{2.5} \text{ or FPM}. \end{cases}$$

$$D_P = \text{representative particle aerodynamic diameter} = \begin{cases} 25\,\mu\text{m for } \text{PM}_{20\text{-}30}, \\ 15\,\mu\text{m for } \text{PM}_{10\text{-}20}, \\ 4\,\mu\text{m for } \text{PM}_{10} \text{ or APM}, \\ 1\,\mu\text{m for } \text{PM}_{2.5} \text{ or FPM}. \end{cases}$$

For aerosol concentrations such as FPM and APM in chemistry mode or for $PM_{2.5}$, PM_{10}, $PM_{10\text{-}20}$ and $PM_{20\text{-}30}$ in dust mode, particle settling in EGM mode is performed using an extra vertical advection term in the prognostic equations for each species, with downward velocity V_S (scaled to be in the terrain-following coordinate system).

Wet deposition in chemistry or dust mode is important only for highly soluble gases and aerosols. For the pollutants considered in this model, the only ones removed by wet processes are SO_2, and H_2O_2, FPM ($PM_{2.5}$), APM (PM_{10}), PM_{20}, and PM_{30}.

For the gases SO_2 and H_2O_2, the amount of each pollutant dissolved in the rain-water fraction of the liquid water is computed for pollutant A as $[A]_R = (L_R RTK_{H\_A})[A]$, where $L_R = q_R\rho/\rho_W$ is the liquid rain-water volume fraction, R is the gas constant (0.082) in atm M^{-1} K^{-1}, T is temperature in K, K_{H_A} is the effective Henry's Law coefficient for A, and concentrations are in ppb. $[A]_R$ is then vertically advected at the speed of the falling rain (V_T), to give $[A]_{R(NEW)}$. The new value of A is then $[A]_{(NEW)} = [A] - [A]_R + [A]_{R(NEW)}$.

For aerosols, the same approach is used as for the gases, except that we assume $K_{H\_A} = K_{H\_MAX} = (L_T RT)^{-1}$ (i.e. that all particles are dissolved in the available water), with the total liquid water volume fraction $L_T = (q_C + q_R)\rho/\rho_W$.

In tracer mode, a number of species with non-zero deposition characteristics can be selected individually for each tracer, with dry deposition characteristics:

SO_2: $r_{water} = 0, r_{soil} = 1000, Sc = \sqrt{64/18}$;

HF: $r_{water} = 0, r_{soil} = 100, Sc = \sqrt{20/18}$.

Both of these species are assumed to be readily dissolved in water, and so totally removed by wet deposition. This assumption for sulfur dioxide is different to that used in chemistry mode, as other species needed to calculate the amount dissolved in the available liquid water (e.g. hydrogen peroxide and ozone) are not available in tracer mode.

3.1.4 Emission correction factors

A range of pollutant emissions types can be used by the model. They include point sources, line sources, area sources and gridded surface sources. TAPM expects the seven optional gridded surface emission files to be in the following forms

- Gridded Surface Emissions (GSE), independent of meteorology;
- Biogenic Surface Emissions (BSE), at T_{vege} = 30°C, PAR = 1000 µmol m^{-2} s^{-1} for VOC, and at T_{soil} = 30°C for NO_X;
- Wood Heater Emissions (WHE), at $T_{screen24}$ = 10°C for all pollutant species;
- Vehicle Petrol eXhaust emissions (VPX), at T_{screen} = 25°C for VOC, NO_X and CO;
- Vehicle Diesel eXhaust emissions (VDX), independent of meteorology;
- Vehicle Lpg eXhaust emissions (VLX), at T_{screen} = 25°C for VOC, NO_X and CO;
- Vehicle Petrol eVaporative emissions (VPV), at T_{screen} = 25°C for VOC;

where T_{vege} is the vegetation temperature (°C), T_{soil} is the soil temperature (°C), PAR is the photo-synthetically active radiation (µmol m^{-2} s^{-1}), $T_{screen24}$ is a running 24-hour screen-level temperature (°C), and T_{screen} is the screen-level temperature (°C). The model adjusts the emissions throughout a simulation, according to predicted temperature and PAR.

The biogenic temperature and radiation corrections are from Guenther et al. (1993) for VOC and from Williams et al. (1992) for NO_X. The wood heater and vehicle temperature corrections used in the model are based on curve-fits to data described by Ng et al. (2000), which for vehicle emissions are based on the US model MOBILE5.

The temperature and radiation corrections for BSE VOC emissions are

VOC:
$$C_T = \frac{\exp\left(\frac{95000(T-303.15)}{303.15RT}\right)}{1+\exp\left(\frac{230000(T-314)}{303.15RT}\right)},$$

$$C_{PAR} = \frac{1.066(0.0027PAR)}{\sqrt{1+(0.0027PAR)^2}},$$

with

$T = T_{vege} + 273.15$,

$R = 8.314$ J K^{-1} mol^{-1},

$PAR = 4.18 \cdot (0.55 \cdot TSR)$ in µmol m^{-2} s^{-1},

TSR = total solar radiation (W m^{-2}).

The temperature correction for BSE NO_X emissions is

NO_X, NO_2: $C_T = \exp(0.071(T-303.15))$,

with $T = T_{soil} + 273.15$.

The temperature correction for WHE emissions for all pollutant species is

$C_T = \max\left(0, 2 - 0.1T_{screen24}\right)$.

The temperature corrections for VPX and VLX emissions are

VOC: $C_T = \begin{cases} 1 - 0.03(T_{screen} - 25), & \text{if } T_{screen} < 25°\text{C} \\ 1 + 0.02(T_{screen} - 25), & \text{if } T_{screen} \geq 25°\text{C} \end{cases}$;

NOX: $C_T = \begin{cases} 1 - 0.0125(T_{screen} - 25), & \text{if } T_{screen} < 25°\text{C} \\ 1 - 0.0025(T_{screen} - 25), & \text{if } T_{screen} \geq 25°\text{C} \end{cases}$;

CO: $C_T = \begin{cases} 1 - 0.02(T_{screen} - 25), & \text{if } T_{screen} < 25°\text{C} \\ 1 + 0.04(T_{screen} - 25), & \text{if } T_{screen} \geq 25°\text{C} \end{cases}$.

The temperature correction for VPV emissions is

VOC: $C_T = \begin{cases} \max\left(0.01, 1 + 0.05\left(\min\left(T_{screen}, 41\right) - 27\right)\right), & \text{if } T_{screen} < 27°\text{C} \\ \max\left(0.01, 1 + 0.20\left(\min\left(T_{screen}, 41\right) - 27\right)\right), & \text{if } T_{screen} \geq 27°\text{C} \end{cases}$.

3.2 Lagrangian particle module

The Lagrangian Particle Module (LPM) can be used on the inner-most nest for selected point sources to allow a more detailed account of near-source effects, including gradual plume rise and near-source dispersion. The LPM uses a PARTPUFF approach as described by Hurley (1994), whereby mass is represented as a puff in the horizontal direction, and as a particle in the vertical direction. This configuration has been used successfully in the Lagrangian Atmospheric Dispersion Model (LADM, Physick et al., 1994). Chemistry is accounted for in a straightforward coupled manner with the EGM, without having to convert secondary pollutant concentration back to particle mass. This is done by tracking primary emissions for a particular source with the LPM and accounting for reactions using the EGM (see later). Deposition processes are neglected in the LPM. Once particles have travelled for a certain length of time (model input), the particle is no longer tracked and its mass is converted to concentration and put onto the EGM grid.

3.2.1 Pollutant equations

In the horizontal directions, particle position is updated through advection by the ambient wind, with diffusion accounted for through a puff width relation based on statistical diffusion theory

$$\frac{d\sigma_y^2}{dt} = 2\left(\sigma_u^2 + \sigma_{up}^2\right)T_{Lu}\left(1 - \exp\left(-\frac{t}{T_{Lu}}\right)\right),$$

where

$\sigma_u^2, \sigma_{up}^2$ are the ambient and plume rise horizontal velocity variances respectively,

$\sigma_u^2 = \min\left(0.01, E - \frac{1}{2}\overline{w'^2}\right)$,

σ_{up}^2 is specified in Section 3.3,

$T_{Lu} = \dfrac{2\sigma_u^2}{C_0\varepsilon}$ is the ambient horizontal Lagrangian timescale,

and $C_0 = 3.0$.

In the vertical direction, particle position is updated using

$$\frac{d\sigma_{particle}}{dt} = \dot{\sigma} + \dot{\sigma}' + \dot{\sigma}'_p,$$

where

$\sigma_{particle}$ is the particle position in terrain following coordinates,

$\dot{\sigma}$ is the mean ambient vertical velocity,

$\dot{\sigma}'$ is the perturbation of vertical velocity due to ambient turbulence,

$\dot{\sigma}'_p$ is the perturbation of vertical velocity due to plume rise effects.

Perfect reflection of particle vertical position and velocity is used at the ground.

The perturbation of vertical velocity due to ambient turbulence is determined from the solution of a Langevin equation using a non-stationary turbulence extension of the approach of Franzese et al. (1999)

$$\dot{\sigma}' = w'\frac{\partial\sigma}{\partial z},$$

$$dw' = (a_0 + a_1 w' + a_2 w'^2)dt + b_0\xi,$$

where ξ is a random number from a Gaussian distribution with mean zero and variance one, and

$$b_0 = \sqrt{C_0\varepsilon dt},$$

$$a_2 = \frac{\frac{1}{3}\left(\frac{\partial\overline{w'^3}}{\partial t} + \frac{\partial\overline{w'^4}}{\partial z}\right) - \frac{\overline{w'^3}}{2\overline{w'^2}}\left(\frac{\partial\overline{w'^2}}{\partial t} + \frac{\partial\overline{w'^3}}{\partial z} - C_0\varepsilon\right) - \overline{w'^2}\,\frac{\partial\overline{w'^2}}{\partial z}}{\overline{w'^4} - \frac{\left(\overline{w'^3}\right)^2}{\overline{w'^2}} - \left(\overline{w'^2}\right)^2},$$

$$a_1 = \frac{1}{2\overline{w'^2}}\left(\frac{\partial\overline{w'^2}}{\partial t} + \frac{\partial\overline{w'^3}}{\partial z} - C_0\varepsilon - 2\overline{w'^3}a_2\right),$$

$$a_0 = \frac{\partial\overline{w'^2}}{\partial z} - \overline{w'^2}a_2.$$

Vertical velocity variance $\overline{w'^2}$ can be diagnosed from the following modified prognostic equation of Gibson and Launder (1978) and Andren (1990), when all advection and diffusion

terms are neglected and the boundary-layer assumption is made (see Mellor and Yamada, 1982),

$$\overline{w'^2} = \left(\tfrac{2}{3} E + \frac{E}{c_{s1}\varepsilon} \left((2 - c_{s2} - c_{w2} \frac{l}{kz}) P_s + (2 - c_{s3} - c_{w3} \frac{l}{kz}) P_b - \tfrac{2}{3} \varepsilon \right) \right) . \left(1 + \frac{c_{w1}}{c_{s1}} \frac{l}{kz} \right)^{-1},$$

with constants from Rodi (1985)

$c_{s1} = 2.20,\ c_{s2} = 1.63,\ c_{s3} = 0.73,\ c_{w1} = 1.00,\ c_{w2} = 0.24,\ c_{w3} = 0.0$.

Higher-order moments of the vertical velocity distribution $\overline{w'^3}$ and $\overline{w'^4}$ are determined from the vertical velocity variance using

$$\overline{w'^3} = 0.8 \left(\max \left(0, \overline{w'^2} - \overline{w_1'^2} \right) \right)^{3/2},$$
$$\overline{w'^4} = 3.5 \left(\overline{w'^2} \right)^2,$$

in the convective boundary layer, and Gaussian values elsewhere

$$\overline{w'^3} = 0.0,$$
$$\overline{w'^4} = 3.0 \left(\overline{w'^2} \right)^2.$$

The subscript 1 here refers to the value of this variable at the first model level (10 m). This parameterisation produces a skewness of zero at the bottom and top of the convective boundary layer, and a peak value of about 0.6 within this layer. These parameterisations agree with measurements in the convective boundary layer as discussed by Luhar et al. (1996).

The perturbation of vertical velocity due to plume rise effects is determined using a random walk approach

$$\dot{\sigma}'_p = \left(w_p + \xi \sigma_{wp} \right) \frac{\partial \sigma}{\partial z},$$

where ξ is a random number from a Gaussian distribution with mean zero and variance one, and plume rise variables w_p and σ_{wp} are defined in Section 3.3.

In order to calculate total pollutant concentration for use in chemistry calculations and time-averaging, particles are converted to concentration at grid points of the EGM using the equation for the concentration increment of a particle at a grid point

$$\Delta\chi = \frac{\Delta m}{2\pi_c \sigma_y^2 \Delta z} \exp\left(-\frac{r^2}{2\sigma_y^2} \right),$$

where

Δm is the particle mass,

σ_y is the standard deviation of horizontal puff width,

Δz is the vertical grid spacing,

r is the horizontal distance from the particle position to the grid point.

3.2.2 Chemistry

In tracer mode, optional chemical decay of a particular pollutant is represented by exponentially decaying particle mass. In chemistry mode, pollutant emissions are converted to particle mass on release from the source, and stored for the variables APM, FPM, SO_2, NO_X, R_{smog}, SP_X and NO_2. Chemistry is accounted for in these variables by the EGM, except for the loss terms in the equation for SO_2, which are handled through an exponential decay of mass with reaction rate $k_{SO2} = k_8[RP] + k_9[H_2O_2] + k_{10}[O_3]$. This reaction is then not computed in the EGM for the LPM component of SO_2. This approach allows the dispersion of the primary emissions of the above variables to be handled with the LPM, and avoids any dependence of the LPM on the EGM, except for the first order reaction rate of SO_2.

The diagnostic solution for the total concentration is then

$$[APM] = [APM]_{LPM} + [APM]_{EGM},$$
$$[FPM] = [FPM]_{LPM} + [FPM]_{EGM},$$
$$[SO_2] = [SO_2]_{LPM} + [SO_2]_{EGM},$$
$$[NO_X] = [NO_X]_{LPM} + [NO_X]_{EGM},$$
$$[R_{smog}] = [R_{smog}]_{LPM} + [R_{smog}]_{EGM},$$
$$[SP_X] = [SP_X]_{LPM} + [SP_X]_{EGM},$$
$$[NO_2] = [NO_2]_{LPM} + [NO_2]_{EGM},$$
$$[RP] = [RP]_{EGM},$$
$$[H_2O_2] = [H_2O_2]_{EGM}.$$

3.3 Plume rise module

The equations for mean plume rise of a point source emission are based on the model of Glendening et al. (1984), as simplified by Hurley and Manins (1995)

$$\frac{dG}{dt} = 2R\left(\alpha w_p^2 + \beta u_a w_p\right),$$
$$\frac{dF}{dt} = -\frac{sM}{u_p}\left(\frac{M}{M_{eff}} u_a + w_p\right),$$
$$\frac{dM}{dt} = F,$$
$$\frac{dx_p}{dt} = u,$$
$$\frac{dy_p}{dt} = v,$$
$$\frac{dz_p}{dt} = w_p,$$

with

$G = \frac{T_a}{T_p} u_p R^2,$

$F = g u_p R^2 \left(1 - \frac{T_a}{T_p}\right),$

$M = \frac{T_a}{T_p} u_p R^2 w_p,$

$w_p = \frac{M}{G},$

$R = \sqrt{\frac{(G + F/g)}{u_p}},$

$u_p = \sqrt{u_a^2 + w_p^2},$

$u_a = \sqrt{u^2 + v^2},$

G, F, M = plume volume, buoyancy, and momentum flux respectively,

R = plume radius (top - hat cross - section),

u, v, w = cartesian x, y, z components of velocity respectively,

T = temperature,

s = ambient buoyancy frequency,

subscript a refers to ambient variables, subscript p refers to plume variables,

$\alpha = 0.1$, $\beta = 0.6$, are vertical plume and bent - over plume entrainment constants respectively,

$\frac{M}{M_{eff}} = \frac{1}{2.25}$, g = gravitational constant ($9.8\ \mathrm{m\ s^{-2}}$).

Initial conditions for these equations are

$$G_o = \frac{T_a}{T_s} w_s R_s^2,\ F_o = N_E g w_s R_s^2 \left(1 - \frac{T_a}{T_s}\right),\ M_o = \frac{T_a}{T_s} w_s^2 R_s^2,\ R_o = \sqrt{\frac{w_s}{\sqrt{u_a^2 + w_s^2}}},$$

where N_E is the user-specified buoyancy enhancement factor (e.g., see Manins et al., 1992, for parameterisations of N_E to handle overlapping plumes from multiple stacks), and subscript s representing stack exit conditions. Stack height is adjusted for stack-tip downwash following Briggs (1973): $h_{sd} = h_s - 4R_s \max\left(0, 1.5 - \frac{w_s}{u_a}\right)$.

Plume rise is terminated when the plume dissipation rate decreases to ambient levels.

Tests of these equations against both the full Glendening and the Briggs (1975) form of the plume rise equations by Hurley and Manins (1995), showed that the above form was just as good as the full Glendening form for all conditions. Our form also collapses to the Briggs form for a bent-over Boussinesq plume, and to the Briggs vertical plume model equations for zero ambient wind. It was also found that for very hot plumes in a bent-over plume situation, the Briggs form was very close to our form, even though the Boussinesq approximation was not strictly valid. This finding is probably due to the rapid decrease of plume temperature excess with travel time.

In the EGM, plume rise for a point source is accounted for by releasing pollutants at the effective source height as calculated by the above equations, with a plume depth that assumes a 2:1 horizontal to vertical plume shape, and that the plume radius for concentration is two-thirds that of the visual radius R above. Pollutant emissions are then distributed uniformly to grid points within the plume depth at the nearest horizontal grid point (assuming plume width is always sub-grid scale).

In the LPM, a gradual plume rise approach is used with a random component that depends on the standard deviation of the vertical velocity due to plume rise effects, and an enhanced horizontal spread. The standard deviations of velocity assume a slightly simplified form of the above equation for *G*, a 2:1 horizontal to vertical plume shape, a plume radius for concentration of two-thirds the visual radius *R*, and a standard deviation half that of the radius. This results in the equations

$$\sigma_{wp} = \frac{\alpha w_p^2 + \beta u_a w_p}{3\sqrt{2} u_p}, \text{ and } \sigma_{up} = 2\sigma_{wp}.$$

3.4 Building wake module

The effect of building wakes on plume rise and dispersion is based on the Plume Rise Model Enhancements (PRIME) approach of Schulman et al. (2000). The PRIME model uses an along-wind coordinate system, and so first each building is transformed to be in this system. Effective building dimensions and cavity and wake dimensions are then calculated for each building and are then used to determine the combined wake meteorology and turbulence. Plume rise is affected by the modified meteorology and turbulence for point sources in both EGM and LPM modes, while dispersion is influenced only for plumes in LPM mode. LPM calculations are done for both the cavity and wake regions, rather than specifying a uniform concentration in the cavity as is done in PRIME.

3.4.1 Transformation to along-wind coordinate system

Using the local horizontal wind components (*u*, *v*) in a Cartesian coordinate system, a point (*x*, *y*) can be rotated to be in an along-wind coordinate system (x', y') by using the transformation

$$x' = (xu - yv)/U \text{ and } y' = (yu - xv)/U, \text{ with } U = \sqrt{u^2 + v^2}.$$

The horizontal coordinates of the building corners are converted to be in the along-wind coordinate system, using the above transformation. Then, after calculating the minimum and maximum corner point coordinate components, the effective building dimensions are calculated as length $L = x'_{\max} - x'_{\min}$ and width $W = y'_{\max} - y'_{\min}$. We then define the origin for this building at the centre of the upwind face of the building $(x'_0, y'_0) = (x'_{\min}, \tfrac{1}{2}(y'_{\min} + y'_{\max}))$.

3.4.2 Building wake dimensions

Given an effective building length (*L*), width (*W*) and height (*H*) in an along-wind coordinate system (*x*, *y*, *z*) (m) with origin at the centre of the up-wind face of the building, a diffusion length scale (*R*) is

$$R = B_S^{2/3} B_L^{1/3}, \text{ with } B_S = \min(H, W) \text{ and } B_L = \min(8B_S, \max(H, W)).$$

The maximum height of the cavity (recirculation zone) is then

$$H_R = \begin{cases} H, \text{if } L > 0.9R \text{ (reattachment)} \\ H + 0.22R, \text{otherwise} \end{cases},$$

and the length of the cavity from the lee-face of the building is

$$L_R = \frac{1.8W}{\left(\max\left(0.3, \min\left(\frac{L}{H}, 3\right)\right)\right)^{0.3}\left(1+0.24\frac{W}{H}\right)}.$$

The cavity height is

$$H_C(x) = \left\{ \begin{array}{l} \left\{ \begin{array}{l} H, \text{ if } 0 < x \le L \\ H\left(1-\left(\frac{x-L}{L_R}\right)^2\right), \text{ if } L < x < L + L_R \end{array} \right\}, \text{ if } L > 0.9R \\ \left\{ \begin{array}{l} H_R + \frac{4(x-0.5R)^2(H-H_R)}{R^2}, \text{ if } 0 < x \le 0.5R \\ H_R\left(1-\frac{(x-0.5R)^2}{(L+L_R-0.5R)^2}\right)^{0.5}, \text{ if } 0.5R < x < L + L_R \end{array} \right\}, \text{ otherwise} \end{array} \right.$$

and the cavity width is

$$W_C(x) = \left\{ \begin{array}{l} \frac{W}{2} + \frac{R}{3} - \frac{(x-R)^2}{3R}, \text{ if } 0 < x \le R \\ \left(\frac{W}{2} + \frac{R}{3}\right)\sqrt{1-\left(\frac{x-R}{L+L_R}\right)^2}, \text{if } R < x < L + L_R \end{array} \right. .$$

The wake height is

$$H_W(x) = 1.2R\left(\frac{x}{R} + \left(\frac{H}{1.2R}\right)^3\right)^{1/3}$$

and the wake width is

$$W_W(x) = \frac{W}{2} + \frac{R}{3}\left(\frac{x}{R}\right)^{1/3}.$$

3.4.3 Building wake meteorology and turbulence

The meteorology and turbulence characteristics described below are used in the calculation of concentration in the following Sections.

Streamline slope over a building is calculated in along-wind coordinates as

$$\left(\frac{dz}{dx}\right)_{wake}(x)=\begin{cases}0, \text{ if } x<-R\\ \dfrac{F_z 2(H_R-H)(x+R)}{R^2}, \text{ if } -R\le x<0\\ \dfrac{F_z 4(H_R-H)(R-2x)}{R^2}, \text{ if } 0\le x<0.5R\\ \dfrac{F_z(H_R-H)(R-2x)}{(L+L_R-0.5R)^2}\left(\dfrac{z}{H}\right)^{0.3}, \text{ if } 0.5R\le x<L+L_R\\ \dfrac{F_z(H_R-H)(R-2(L+L_R))}{(L+L_R-0.5R)^2}\left(\dfrac{z}{H}\right)^{0.3}\left(\dfrac{L+L_R}{x}\right), \text{ if } x\ge L+L_R\end{cases}$$

with $F_z=1$ if $z\le H$, and if $z>H$ then

$$F_z=\begin{cases}1, \text{ if } x<-R\\ \left(\dfrac{H}{z}\right)^3, \text{ if } -R\le x<0.5R.\\ \left(\dfrac{H}{z}\right), \text{ if } x\ge R\end{cases}$$

The horizontal wind speed factor F_U and the turbulence intensities i_x and i_z are calculated as follows.

If $x\le L+L_R$ and $z\le H_R$

$$F_U=F_C,$$

$$F_C=\max\left(0.1,1-\frac{\frac{\Delta U}{U}H_W}{0.5(H_C+H_W)}\right),$$

$$i_z=i_{zc}/\left(1-\tfrac{\Delta U}{U}\right),$$

$$i_x=0.5\max\left(0.3,\min\left(\tfrac{W}{H},3\right)\right),$$

otherwise if $z\le H_W$

$$F_U=F_C+(1-F_C)\frac{(z-H_C)}{(H_W-H_C)},$$

$$F_C=\max\left(0.1,1-\frac{F_x\frac{\Delta U}{U}H_W}{0.5(H_C+H_W)}\right),$$

$$i_z=1.7i_{zN}\left(\frac{F_x}{1-F_x\frac{\Delta U}{U}}\right),$$

$$i_x=i_z,$$

$$F_x = \begin{cases} \left(\frac{x}{L}\right)^{2/3}, \text{ if } 0 < x < L \\ \left(\frac{R}{x - L + R}\right)^{2/3}, \text{ if } x \geq L \end{cases},$$

with $\frac{\Delta U}{U} = 0.7$, $i_{zc} = 0.65$ and $i_{zN} = 0.06$.

Note that we have parameterised cavity turbulence, and do not assume a uniform cavity concentration as is done in PRIME. Note also that wake calculations are done only if $x < 15R$ and $|y| < 0.5W_W$.

3.4.4 Treatment of multiple building blocks

If we define a building block as having a constant height *H*, then we can use the above procedure to define wake characteristics for each building block. The effects of overlapping wakes from multiple building blocks, whether from the same multi-level or multi-tiered physical building, or from multiple physical buildings, can be treated by combining the meteorology and turbulence. For a particular point in space, the combined (for all building blocks)

- streamline slope can be calculated by first calculating the maximum slope and the minimum slope, and then if the absolute value of the maximum is greater than the absolute value of the minimum, then use the maximum value, otherwise use the minimum value;
- horizontal wind speed factor is the minimum value;
- turbulence intensity is the maximum value.

The combined effects can then be used for the calculation of plume rise and dispersion – the above approach attempts to be conservative for expected ground-level pollution concentration.

3.4.5 Wake effects on plume rise

For the calculation of plume rise (Section 3.3), the horizontal wind and the differential equations for *G* and z_p are adjusted as follows

$u = u_{old} F_U$, $v = v_{old} F_U$ and then $U = \sqrt{u^2 + v^2}$,

$$\frac{dG}{dt} = \max\left(\left.\frac{dG}{dt}\right|_{old}, \sqrt{\frac{\pi_c}{2}} U^2 i_z\right),$$

$$\frac{dz_p}{dt} = \left.\frac{dz_p}{dt}\right|_{old} + U\left(\frac{dz}{dx}\right)_{wake}.$$

3.4.6 Wake effects on LPM dispersion

For LPM dispersion, the mean wind is modified

$u = u_{old} F_U$, $v = v_{old} F_U$ and then $U = \sqrt{u^2 + v^2}$, and $w = w_{old} + U\left(\frac{dz}{dx}\right)_{wake}$,

while the horizontal plume spread incorporates an extra term using $\sigma_u = Ui_x$ and the LPM random-walk equation also includes a contribution from $\sigma_w = Ui_z$.

3.4.7 Wake effects on EGM dispersion

The influence of building wakes on dispersion in EGM mode allows them to be included not only for point sources, but also for line, area/volume and gridded emission sources. The approach taken is to modify the mean and turbulence fields from those predicted with the meteorological module, by using the same corrections for building wake meteorology and turbulence as above, based on the PRIME parameterisations.

For EGM dispersion, the mean wind is modified

$u = u_{old} F_U$, $v = v_{old} F_U$ and then $U = \sqrt{u^2 + v^2}$, and $w = w_{old} + U\left(\frac{dz}{dx}\right)_{wake}$,

while the turbulence is modified

$$E = E_{old} + E_{wake}$$
$$\varepsilon = \varepsilon_{old} + \varepsilon_{wake}$$

with

$$E_{wake} \equiv \sigma_u^2 + \tfrac{1}{2}\sigma_w^2 = (Ui_x)^2 + \tfrac{1}{2}(Ui_z)^2$$
$$\varepsilon_{wake} = c_m^{3/4} \frac{E_{wake}^{3/2}}{H_w} \quad .$$

Note that here the value of H_w is the maximum of the building wake heights at a particular point, when there are multiple buildings. The diffusion coefficient is calculated using E and ε above, using the standard definition.

4 Numerical methods

The flow chart in Figure 1 illustrates the order of calculations in the model. The model uses a large timestep of 300 s on which radiation and surface processes are calculated. Meteorological and turbulence equations are solved with a timestep of $\Delta t_M = \frac{1}{U_M}\min(\Delta x_M, \Delta y_M)$, where U_M is a characteristic wind speed (U_M = 30 m s^{-1} is the model default), and Δx_M and Δy_M are the horizontal grid spacings in metres on the meteorological grid. Pollution concentration equations for the EGM are solved with a timestep of $\Delta t_P = \frac{1}{U_P}\min(\Delta x_P, \Delta y_P)$, where $U_P = 0.5U_M$, and Δx_P and Δy_P are the horizontal grid spacings in metres on the pollution grid. The pollution grid can be a subset of the meteorological grid at finer grid spacing. The maximum synoptic wind speed used by the model is set to be U_M, in order to avoid Courant numbers being too much greater than 1 for the meteorology. This restriction was found to be important for the reduction of numerical error, particularly near the model top and in non-hydrostatic mode.

Model equations are solved using finite difference methods with no grid stagger, a constant grid spacing in the horizontal directions, and a variable grid spacing in the vertical direction. Second-order centred spatial differencing is used, for example

$$\left.\frac{\partial\phi}{\partial x}\right|_i = \frac{1}{2\Delta x}(\phi_{i+1} - \phi_{i-1}),$$

$$\left.\frac{\partial\phi}{\partial y}\right|_j = \frac{1}{2\Delta y}(\phi_{j+1} - \phi_{j-1}),$$

$$\left.\frac{\partial\phi}{\partial\sigma}\right|_k = \frac{1}{(\sigma_{k+1} - \sigma_{k-1})}\left(\left(\frac{\sigma_k - \sigma_{k-1}}{\sigma_{k+1} - \sigma_k}\right)(\phi_{k+1} - \phi_k) + \left(\frac{\sigma_{k+1} - \sigma_k}{\sigma_k - \sigma_{k-1}}\right)(\phi_k - \phi_{k-1})\right),$$

$$\left.\frac{\partial}{\partial x}\left(K\frac{\partial\phi}{\partial x}\right)\right|_i = \frac{1}{2(\Delta x)^2}\left((K_{i+1} + K_i)(\phi_{i+1} - \phi_i) - (K_i + K_{i-1})(\phi_i - \phi_{i-1})\right),$$

$$\left.\frac{\partial}{\partial y}\left(K\frac{\partial\phi}{\partial y}\right)\right|_j = \frac{1}{2(\Delta y)^2}\left((K_{j+1} + K_j)(\phi_{j+1} - \phi_j) - (K_j + K_{j-1})(\phi_j - \phi_{j-1})\right),$$

$$\left.\frac{\partial}{\partial\sigma}\left(K\frac{\partial\phi}{\partial\sigma}\right)\right|_k = \frac{1}{(\sigma_{k+1} - \sigma_{k-1})}\left(\left(\frac{K_{k+1} + K_k}{\sigma_{k+1} - \sigma_k}\right)(\phi_{k+1} - \phi_k) - \left(\frac{K_k + K_{k-1}}{\sigma_k - \sigma_{k-1}}\right)(\phi_k - \phi_{k-1})\right).$$

4.1 Horizontal advection

Horizontal advection for all prognostic variables is calculated with timesteps Δt_M or Δt_P using the semi-Lagrangian technique of McGregor (1993) with the quasi-monotone conversion of Bermejo and Staniforth (1992). To $O((\Delta t)^2)$, the departure point (i_*, j_*) in grid units can be determined for horizontal grid point (i, j) from

$$i_* = i - u_{i,j}^{n+1/2}\frac{\Delta t}{\Delta x} + \frac{(\Delta t)^2}{2\Delta x}\left(u\frac{\partial u}{\partial x} + v\frac{\partial u}{\partial y}\right)\Bigg|_{i,j}^{n+1/2},$$

$$j_* = j - v_{i,j}^{n+1/2}\frac{\Delta t}{\Delta y} + \frac{(\Delta t)^2}{2\Delta y}\left(u\frac{\partial u}{\partial x} + v\frac{\partial u}{\partial y}\right)\Bigg|_{i,j}^{n+1/2},$$

with $u_{i,j}^{n+1/2} = 1.5u_{i,j}^n - 0.5u_{i,j}^{n-1}$ or $u_{i,j}^{n+f} = fu_{i,j}^{n+1} + (1-f)u_{i,j}^n$ and similarly for v**,** for the meteorological and concentration variables respectively (f accounts for fractional timesteps). Each prognostic variable can then be determined from $\phi_{i,j}^{n+1} = \phi_{i_*,j_*}^n$ using Lagrange cubic polynomial interpolation separately in each coordinate direction.

Defining $i = \text{int}(i_*)$ and $x_* = i_* - i$, then

$$\phi_{i_*j}^n = -\tfrac{1}{6}x_*(x_* - 1)(x_* - 2)\phi_{i-1\,j}^n + \tfrac{1}{2}(x_*^2 - 1)(x_* - 2)\phi_{ij}^n$$
$$-\tfrac{1}{2}x_*(x_* + 1)(x_* - 2)\phi_{i+1\,j}^n + \tfrac{1}{6}x_*(x_*^2 - 1)\phi_{i+2\,j}^n,$$

subject to $\min(\phi_{ij}^n, \phi_{i+1\,j}^n) \le \phi_{i_*j}^n \le \max(\phi_{ij}^n, \phi_{i+1\,j}^n)$.

Similarly, if $j = \text{int}(j_*)$ and $y_* = j_* - j$, then

$$\phi_{i_*j_*}^n = -\tfrac{1}{6}y_*(y_* - 1)(y_* - 2)\phi_{i_*j-1}^n + \tfrac{1}{2}(y_*^2 - 1)(y_* - 2)\phi_{i_*j}^n$$
$$-\tfrac{1}{2}y_*(y_* + 1)(y_* - 2)\phi_{i_*j+1}^n + \tfrac{1}{6}y_*(y_*^2 - 1)\phi_{i_*j+2}^n,$$

subject to $\min(\phi_{i_*j}^n, \phi_{i_*j+1}^n) \le \phi_{i_*j_*}^n \le \max(\phi_{i_*j}^n, \phi_{i_*j+1}^n)$.

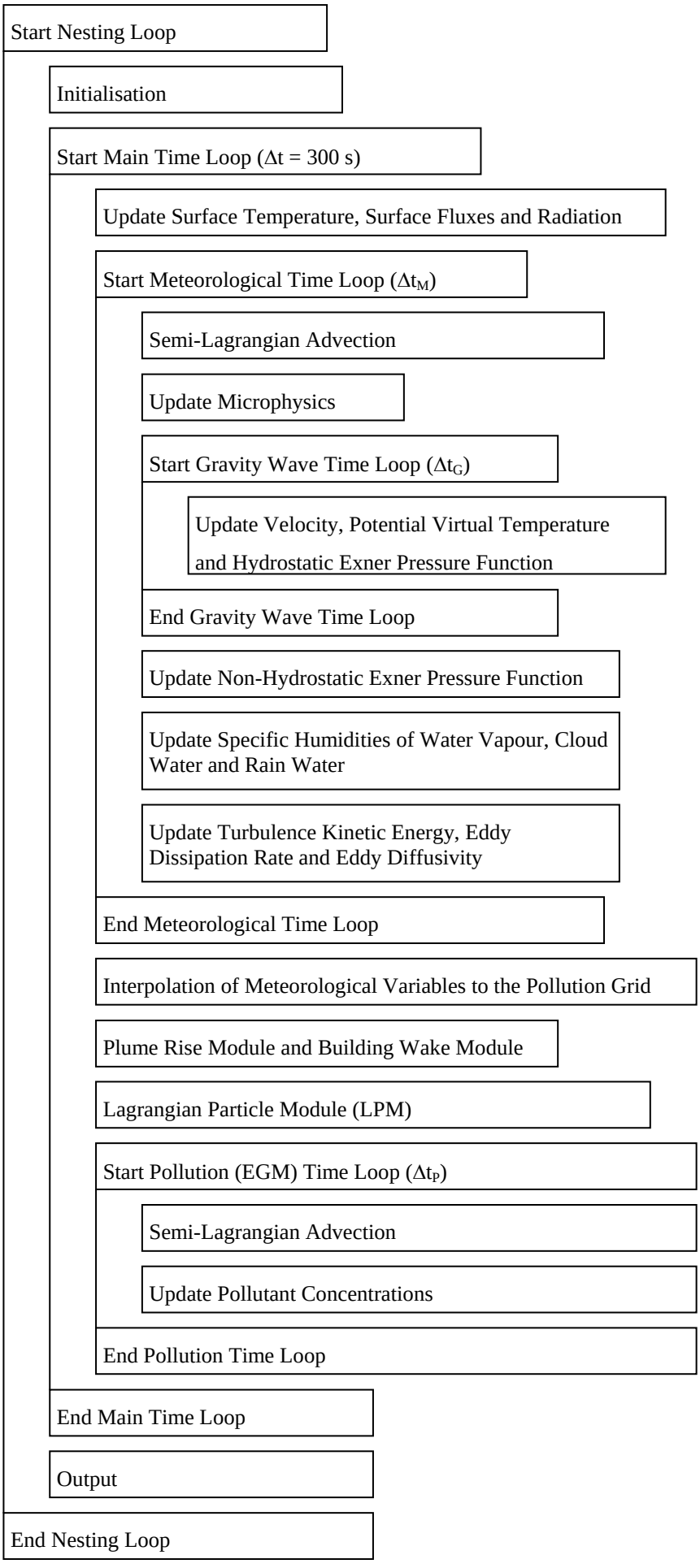

Figure 1. Flow chart of TAPM.

4.2 Vertical advection

Vertical advection for all prognostic variables except θ_v, is calculated with timesteps Δt_M or Δt_P using the semi-Lagrangian technique of McGregor (1993) with the quasi-monotone conversion of Bermejo and Staniforth (1992). To $O((\Delta t)^2)$, the departure point can be determined from

$$\sigma_* = \sigma_k - \dot{\sigma}_k^{n+1/2}\Delta t + \tfrac{1}{2}(\Delta t)^2\left(\dot{\sigma}\frac{\partial\dot{\sigma}}{\partial\sigma}\right)\Bigg|_k^{n+1/2},$$

with $\dot{\sigma}_k^{n+1/2} = 1.5\dot{\sigma}_k^n - 0.5\dot{\sigma}_k^{n-1}$ or $\dot{\sigma}_k^{n+f} = f\dot{\sigma}_k^{n+1} + (1-f)\dot{\sigma}_k^n$, for the meteorological and concentration variables respectively (*f* accounts for fractional timesteps). Each prognostic variable can then be determined from $\phi_k^{n+1} = \phi_{k_*}^n$ (where *k* denotes the nearest model level to σ_* that satisfies $\sigma_k \le \sigma_*$), using Lagrange cubic polynomial interpolation (with quasi-monotone conversion)

$$\begin{aligned}\phi_{k_*}^n = &\left(\frac{\sigma_*-\sigma_k}{\sigma_{k-1}-\sigma_k}\right)\left(\frac{\sigma_*-\sigma_{k+1}}{\sigma_{k-1}-\sigma_{k+1}}\right)\left(\frac{\sigma_*-\sigma_{k+2}}{\sigma_{k-1}-\sigma_{k+2}}\right)\phi_{k-1}^n\\ &+\left(\frac{\sigma_*-\sigma_{k-1}}{\sigma_k-\sigma_{k-1}}\right)\left(\frac{\sigma_*-\sigma_{k+1}}{\sigma_k-\sigma_{k+1}}\right)\left(\frac{\sigma_*-\sigma_{k+2}}{\sigma_k-\sigma_{k+2}}\right)\phi_k^n\\ &+\left(\frac{\sigma_*-\sigma_{k-1}}{\sigma_{k+1}-\sigma_{k-1}}\right)\left(\frac{\sigma_*-\sigma_k}{\sigma_{k+1}-\sigma_k}\right)\left(\frac{\sigma_*-\sigma_{k+2}}{\sigma_{k+1}-\sigma_{k+2}}\right)\phi_{k+1}^n\\ &+\left(\frac{\sigma_*-\sigma_{k-1}}{\sigma_{k+2}-\sigma_{k-1}}\right)\left(\frac{\sigma_*-\sigma_k}{\sigma_{k+2}-\sigma_k}\right)\left(\frac{\sigma_*-\sigma_{k+1}}{\sigma_{k+2}-\sigma_{k+1}}\right)\phi_{k+2}^n,\end{aligned}$$

subject to $\min(\phi_k^n, \phi_{k+1}^n) \le \phi_{k_*}^n \le \max(\phi_k^n, \phi_{k+1}^n)$.

4.3 Gravity waves

The equations for the meteorological variables $u, v, \dot{\sigma}, \theta_v$, and π_H are solved by using a time-split approach where gravity wave terms are separated from the others and solved on a small timestep $\Delta t_G = \frac{1}{U_G}\min(\Delta x_M, \Delta y_M)$, where U_G = 120 m s^{-1} (note that U_G = 140 m s^{-1} for grid spacing below 1000 m)

$$\frac{\partial u}{\partial t} = -\theta_v\frac{\partial \pi_H}{\partial x} + R_u,$$

$$\frac{\partial v}{\partial t} = -\theta_v\frac{\partial \pi_H}{\partial y} + R_v,$$

$$\frac{\partial\dot{\sigma}}{\partial\sigma} = -\left(\frac{\partial u}{\partial x}+\frac{\partial v}{\partial y}\right) + u\frac{\partial^2\sigma}{\partial\sigma\partial x} + v\frac{\partial^2\sigma}{\partial\sigma\partial y},$$

$$\frac{\partial \theta_v}{\partial t} = -\dot{\sigma}\frac{\partial \theta_v}{\partial \sigma} + R_{\theta_v},$$

$$\frac{\partial \pi_H}{\partial \sigma} = -\frac{g}{\theta_v}\left(\frac{\partial \sigma}{\partial z}\right)^{-1},$$

with R_u, R_v, and R_{θ_v} (updated on the timestep Δt_M)

$$R_u = g\frac{\partial \sigma}{\partial x}\left(\frac{\partial \sigma}{\partial z}\right)^{-1} + f(v - v_s) - N_s(u - u_s) - \theta_v\left(\frac{\partial \pi_N}{\partial x} + \frac{\partial \pi_N}{\partial \sigma}\frac{\partial \sigma}{\partial x}\right),$$

$$R_v = g\frac{\partial \sigma}{\partial y}\left(\frac{\partial \sigma}{\partial z}\right)^{-1} - f(u - u_s) - N_s(v - v_s) - \theta_v\left(\frac{\partial \pi_N}{\partial y} + \frac{\partial \pi_N}{\partial \sigma}\frac{\partial \sigma}{\partial y}\right),$$

$$R_{\theta_v} = S_{\theta_v} - \gamma_{cg}\frac{\partial K}{\partial \sigma}\frac{\partial \sigma}{\partial z} - N_s(\theta_v - \theta_{vs}),$$

and also include the nesting terms.

Note that the gravity wave time-step is also linked to the user-selectable maximum synoptic wind speed parameter, similar to the approach used to control the advection time-step. This means that if the maximum synoptic wind speed parameter is selected to be greater than U_M = 30 m s^{-1}, then as well as decreasing the advection time-step, the gravity wave time step will also be decreased.

These prognostic equations are solved using the second-order Adams-Bashforth scheme

$$u^{n+1} = u^n + \frac{\Delta t}{2}\left(3\frac{\partial u}{\partial t}\bigg|^n - \frac{\partial u}{\partial t}\bigg|^{n-1}\right),$$

while diagnostic vertical integration using the trapezoidal rule is performed from the ground to the model top to obtain $\dot{\sigma}$, and from the model top to the ground to obtain π_H.

On the timestep Δt_G, an implicit tri-diagonal horizontal filter described by Pielke (1984) is used. The filter, represented by $F(\phi)$ in equations 1, 2 and 4 of Section 2.1, is applied separately in each horizontal direction with a filter coefficient of δ = 0.10 (increased values are used near the top of the model). The equations solved are

$$(1-\delta)\phi_{i-1j}^{n+1} + 2(1+\delta)\phi_{ij}^{n+1} + (1-\delta)\phi_{i+1j}^{n+1} = \phi_{i-1j}^{n} + 2\phi_{ij}^{n} + \phi_{i+1j}^{n},$$

$$(1-\delta)\phi_{ij-1}^{n+1} + 2(1+\delta)\phi_{ij}^{n+1} + (1-\delta)\phi_{ij+1}^{n+1} = \phi_{ij-1}^{n} + 2\phi_{ij}^{n} + \phi_{ij+1}^{n}.$$

On the timestep Δt_M, vertical diffusion is solved using a first-order implicit approach with special treatment of fluxes at the surface boundary (see next section).

4.4 Scalar prognostic equations

All other prognostic equations including those for specific humidity, turbulence, and pollutant concentrations, are of the general form for variable χ

$$\frac{\partial \chi}{\partial t} = \left(\frac{\partial \sigma}{\partial z}\right)^2 \frac{\partial}{\partial \sigma}\left(K\frac{\partial \chi}{\partial \sigma}\right) + RHS_1 - \chi RHS_2.$$

This equation is solved using first-order time differencing with a semi-implicit approach to give the equation

$$(1+\Delta t RHS_2)\chi^{n+1} - \Delta t\left(\frac{\partial\sigma}{\partial z}\right)^2 \frac{\partial}{\partial\sigma}\left(K\frac{\partial\chi^{n+1}}{\partial\sigma}\right) = \chi^n + \Delta t RHS_1,$$

which can be solved as follows (with special treatment of fluxes at the surface) using a tri-diagonal solution method if second-order spatial differencing is used

$$A\chi_{k-1}^{n+1} + B\chi_k^{n+1} + C\chi_{k+1}^{n+1} = D;$$

if $k > 1$:

$$A = -\left(\frac{\partial\sigma}{\partial z}\right)^2 \frac{\Delta t}{(\sigma_{k+1}-\sigma_{k-1})}\left(\frac{K_k + K_{k-1}}{\sigma_k - \sigma_{k-1}}\right),$$

$$C = -\left(\frac{\partial\sigma}{\partial z}\right)^2 \frac{\Delta t}{(\sigma_{k+1}-\sigma_{k-1})}\left(\frac{K_{k+1} + K_k}{\sigma_{k+1} - \sigma_k}\right),$$

$$B = 1 + \Delta t RHS_2 - A - C,$$

$$D = \chi_k^n + \Delta t RHS_1;$$

if $k = 1$:

$$A = 0,$$

$$C = -\frac{1}{2}\left(\frac{\partial\sigma}{\partial z}\right)^2 \frac{\Delta t}{(\sigma_{3/2}-\sigma_0)}\left(\frac{K_2 + K_1}{\sigma_2 - \sigma_1}\right),$$

$$B = 1 + \Delta t RHS_2 - C,$$

$$D = \chi_1^n + \Delta t RHS_1 - \Delta t\left(\frac{\partial\sigma}{\partial z}\right)\frac{\text{flux}(\chi)}{(\sigma_{3/2}-\sigma_0)},$$

with $\text{flux}(\chi) = u_*\chi_*$ or $\text{flux}(\chi) = V_d\chi_1$.

The value of RHS_2 is non-zero only for the ε equation, the $\overline{\theta_v'\chi'}$ equations, and the SO_2, NO_2, RP and H_2O_2 pollutant concentration equations, where the loss terms are treated implicitly. The RHS_1 term includes all other terms in the particular prognostic equations, including explicit horizontal diffusion. The non-zero RHS_2 terms are

$$\varepsilon: RHS_2 = c_{\varepsilon 2}\frac{\varepsilon}{E},$$

$$\overline{\theta_v'\chi'}: RHS_2 = \frac{2}{c_\chi}\frac{\varepsilon}{E},$$

$$[SO_2]: RHS_2 = k_8[RP] + k_9[H_2O_2] + k_{10}[O_3],$$

$$[NO_2]: RHS_2 = k_3 + k_4([NO_X] + [SP_X] - [NO_2]),$$

$$[RP]: RHS_2 = k_2[NO] + k_5[RP] + (k_6 + k_7)[NO_2] + k_8[SO_2],$$

$$[H_2O_2]: RHS_2 = k_9[SO_2].$$

When the stability criterion for explicit horizontal diffusion of pollution variables is breached, the solution dynamically switches to an unconditionally stable implicit mode analogous to that used for vertical diffusion.

4.5 Other methods

- On the timestep Δt_M, the elliptic non-hydrostatic pressure perturbation equation is solved using an iterative approach. The solution is performed only for a sub-grid region that excludes the 5 edge grid points at the top and lateral boundaries, as these edge regions usually contain noisy solutions which can produce spurious vertical velocities to which the non-hydrostatic solution is highly sensitive.
- For numerical representation of the vertical fluxes, it is necessary to use a finite difference approximation consistent with that used for the vertical diffusion

$$\overline{w'\chi'}\Big|_k = -\tfrac{1}{2}(K_{k+1}+K_k)\left(\frac{\sigma_k-\sigma_{k-1}}{\sigma_{k+1}-\sigma_{k-1}}\right)\left(\frac{\chi_{k+1}-\chi_k}{\sigma_{k+1}-\sigma_k}\right)\left(\frac{\partial\sigma}{\partial z}\right)$$
$$-\tfrac{1}{2}(K_k+K_{k-1})\left(\frac{\sigma_{k+1}-\sigma_k}{\sigma_{k+1}-\sigma_{k-1}}\right)\left(\frac{\chi_k-\chi_{k-1}}{\sigma_k-\sigma_{k-1}}\right)\left(\frac{\partial\sigma}{\partial z}\right).$$

- At times of rapid variations in the surface temperature and specific humidity (such as just after sunrise), the surface heat balance approach used for vegetation can produce oscillations. Therefore, the vegetation temperature and moisture are time averaged using the current and previous values to prevent the oscillations.
- Linear interpolation is used to convert the synoptic-scale variables from the gridded analyses to the model.
- The plume rise equations are solved using the fourth-order Runge-Kutta method with a timestep of 1 second.
- The LPM uses explicit, forward in time finite differences and centred in space finite differences, with a large timestep of $\Delta t_{LPM} = 2\Delta t_P$ and a small timestep of 5 seconds for the solution in the vertical direction.
- The turbulence production/dissipation balance and wet processes are handled separately on a small timestep of 100 s.
- For multi-dimensional simulations, it was found necessary to bound the value of the length scale in order to keep the numerical solution stable for the ε prognostic equation. Also, the counter-gradient tracer flux and cross-correlation term are restricted to be zero in thermally stable regions, and are bounded elsewhere.

5 Acknowledgments

Some of the methodologies and parameterisations used in TAPM were also used in the Lagrangian Atmospheric Dispersion Model (LADM) of Physick et al. (1994), and experience gained by working with other team members on developing and applying LADM was invaluable in the development of TAPM.

The encouragement, advice and suggestions for improvements from Bill Physick, Mary Edwards, Peter Manins, Mark Hibberd, Ashok Luhar, Julie Noonan and Martin Cope on TAPM is much appreciated. Helpful comments from many other people in CSIRO Atmospheric Research and CSIRO Energy Technology on various aspects of this work, including the implementation of some of the model parameterisations, are gratefully acknowledged. The suggestions for improving/extending TAPM by model users has also been invaluable in the development of TAPM.

6 References

Andren A. (1990). 'Evaluation of a turbulence closure scheme suitable for air pollution applications', *J. Appl. Meteorol.*, **29**, 224-239.

Azzi M., Johnson G.M., and Cope M. (1992). 'An introduction to the generic reaction set photochemical smog mechanism', *Proceedings of the 11th International Clean Air and Environment Conference*, Brisbane, 1992, Clean Air Society of Australia & New Zealand.

Bermejo R., and Staniforth A. (1992). 'The conversion of semi-Lagrangian schemes to quasi-monotone schemes', *Mon. Wea. Rev.* **120**, 2622-2632.

Briggs G.A. (1973). 'Diffusion estimation for small emissions', ATDL No 79, Atmospheric Turbulent Diffusion Laboratory, NOAA Environmental Resources Laboratory, Oak Ridge, Tennessee.

Briggs G.A. (1975). 'Plume Rise Predictions. In *Lectures on Air Pollution and Environmental Impact Analysis*', Ed. D.A. Haugen, AMS, Boston, MA, pp. 59-111.

Davies H. (1976). 'A lateral boundary formulation for multi-level prediction models', *Q. J. R. Meteorol. Soc*. **102**, 405-418.

Deardorff J.W. (1966). 'The counter-gradient heat flux in the lower atmosphere and in the laboratory', *J. Atmos. Sci.*, **23**, 503-506.

Derbyshire S.H. (1990). 'Nieuwstadt's stable boundary layer revisited', *Q. J. R. Meteorol. Soc*. **116**, 127-158.

Dilley A.C., and O'Brien D.M. (1999). 'Estimating downward clear-sky long-wave irradiance at the surface from screen temperature and precipitable water', *Submitted to Q. J. R. Meteorol. Soc.*

Duynkerke P.G. (1988). 'Application of the E-ε turbulence closure model to the neutral and stable atmospheric boundary layer', *J. Atmos. Sci.*, **45**, 865-880.

Duynkerke P.G., and Driedonks A.G.M. (1987). 'A model for the turbulent structure of the stratocumulus-topped atmospheric boundary layer', *J. Atmos. Sci.*, **44**, 43-64.

Dyer A.J., and Hicks B.B. (1970). 'Flux-gradient relationships in the constant flux layer', *Quart. J. Roy. Meteorol. Soc.*, **96**, 715-721.

Enger L. (1986). 'A higher order closure model applied to dispersion in a convective pbl', *Atmos. Environ.*, **20**, 879-894.

Franzese P., Luhar A.K., and Borgas M.S. (1999). 'An efficient Lagrangian stochastic model of vertical dispersion in the convective boundary layer.' *Atmos. Environ.*, **33**, 2337-2345.

Garratt J.R. (1992). 'The atmospheric boundary layer', Cambridge atmospheric and space science series, Cambridge University Press, Cambridge, 316 pp.

Gibson M.M., and Launder B.E. (1978). 'Ground effects on pressure fluctuations in the atmospheric boundary layer', *J. Fluid Mech.*, **86**, 491-511.

Glendening J.W., Businger J.A., and Farber R.J. (1984). 'Improving Plume Rise Prediction Accuracy for Stable Atmospheres with Complex Vertical Structure', *J. Air Pollut. Control Ass.*, **34**, pp. 1128-1133.

Guenther A., Zimmerman P., Harley P., Monson R. and Fall R. (1993). 'Isoprene and monoterpene emission rate variability: Model evaluations and sensitivity analyses.' *J. Geophys. Res.*, **98**, 12609-12617.

Harley R.A., Russell A.G., McRae G.J., Cass G.R. & Seinfeld J.H. (1993). 'Photochemical modelling of the southern California air quality study', *Environ. Sci. Technol.*, **27**, 378-388.

Hurley, P.J. (1994). 'PARTPUFF - A Lagrangian particle/puff approach for plume dispersion modelling applications', *J. Appl. Meteorol.*, **33**, 285-294.

Hurley P.J., and Manins P.C. (1995). 'Plume rise and enhanced dispersion in LADM'. CSIRO Atmospheric Research, ECRU Technical Note No. 4. 4 pp.

Hurley P., Physick W., Cope M., Borgas M., Brace P. (2003). 'An evaluation of TAPM for photochemical smog applications in the Pilbara region of WA', *Proceedings of the National Clean Air Conference of CASANZ*, Newcastle, Australia, 23-27 November 2003.

Hurley P., Physick W., Luhar A. and Edwards M. (2005). 'The Air Pollution Model (TAPM) Version 3. Part 2: Summary of some verification studies', CSIRO Atmospheric Research Technical Paper No. 72. 36 pp.

Johnson G.M. (1984). 'A simple model for predicting the ozone concentration of ambient air', *Proceedings of the 8th International Clean Air and Environment Conference*, New Zealand, 1984, Clean Air Society of Australia & New Zealand.

Katzfey J.J., and Ryan B.F. (1997). 'Modification of the thermodynamic structure of the lower Troposphere by the evaporation of precipitation: A GEWEX cloud system study', *Mon. Wea. Rev.*, **125**, 1431-1446.

Kowalczyk E.A., Garratt J.R., and Krummel P.B. (1991). 'A soil-canopy scheme for use in a numerical model of the atmosphere - 1D stand alone model', CSIRO Atmospheric Research Technical Paper No. 23. 56 pp.

Lin Y., Farley R., and Orville H. (1983). 'Bulk parameterisation of the snow field in a cloud model', *J. Cli. & App. Meteor.*, **22**, 1065–1092.

Luhar A.K., Hibberd M.F., and Hurley P.J. (1996). 'Comparison of Closure Schemes used to Specify the Velocity PDF in Lagrangian Stochastic Dispersion Models for Convective Conditions.' *Atmos. Environ.*, **30**, 1407-1418.

Mahrer Y., and Pielke R.A. (1977). 'A numerical study of the airflow over irregular terrain', *Beitr. Phys. Atmosph.*, **50**, 98-113.

Manins P., Carras J. and Williams D. (1992). 'Plume rise from multiple stacks', *Clean Air*, **26**, 65-68.

McGregor J. (1993). 'Economical determination of departure points for semi-Lagrangian Models', *Mon. Wea. Rev.* **121**, 221-230.

Mellor G.L., and Yamada T. (1982) 'Development of a turbulence closure model for geophysical fluid problems', *Rev. Geophys. Space Phys.*, **20**, 851-875.

Ng Y., Serebryanikova R. and Wong L. (2000). 'Application of the emissions modelling system EMS-95 to the Victorian Inventory', *Proceedings of the 15th International Clean Air Conference of CASANZ,* Sydney, 26-30 November 2000.

Oke T.R. (1988). 'The urban energy balance', *Progress in Physical Geography*, **12**, 471-508.

Physick W.L. (1994). 'Calculation of dry deposition in LADM', CSIRO Atmospheric Research ECRU Technical Note No. 1.

Physick W.L., Noonan J.A., McGregor J.L., Hurley P.J., Abbs D.J., and Manins P.C. (1994). 'LADM: A Lagrangian Atmospheric Dispersion Model', CSIRO Atmospheric Research Technical Paper No. 24. 137 pp.

Pielke R.A. (1984). 'Mesoscale Meteorological modelling', Academic Press, Orlando, 612 pp.

Rodi W. (1985). 'Calculation of stably stratified shear-layer flows with a buoyancy-extended k-ε turbulence model', in J.C.R. Hunt (ed.), *Turbulence and diffusion in stable environments*, Clarendon Press, Oxford, 111-143.

Rotstayn L. (1997). 'A physically based scheme for the treatment of stratiform clouds and precipitation in large scale models. I: Description and evaluation of the microphysical processes', *Quart. J. Roy. Meteor. Soc.*, **123**, 1227–1282.

Ryan B. (2002). 'A bulk parameterisation of the ice particle size distribution and the optical properties in ice clouds', *J. Atmos. Sci.*, **57**, 1436–1451.

Schulman L., Strimaitis D. and Scire J. (2000). 'Development and evaluation of the PRIME plume rise and building downwash model', *J. Air & Waste Manage. Assoc.*, **50**, 378-390.

Seinfeld J.H., and Pandis S.N. (1998). 'Atmospheric chemistry and physics from air pollution to climate change', Wiley, New York, 1326 pp.

Stauffer D.R., and Seaman N.L. (1994). 'Multiscale four-dimensional data assimilation', *Journal of Applied Meteorology*, **33**, 416-434.

Stephens G.L. (1978). 'Radiation profiles in extended water clouds II : Parameterisation schemes'. *J. Atmos. Sci.*, **35**, 2123-2132.

Tripoli G., and Cotton W. (1980). 'A numerical investigation of several factors contributing to the observed variable intensity of deep convection over south Florida', *J. App. Meteor.*, **19**, 1037–1063.

Venkatram A., Karamchandani P., Prasad P., Sloane C., Saxena P., and Goldstein R. (1997). 'The development of a model to examine source-receptor relationships for visibility on the Colorado Plateau', *Journal of the Air and Waste Management Association*, **47**, 286-301.

Wesley M.L. (1989). 'Parameterisation of surface resistances to gaseous dry deposition in regional-scale numerical models', *Atmos. Environ.*, **23**, 1293-1304.

Williams E., Guenther A., and Fehsenfeld F. (1992). 'An inventory of nitric oxide emissions from soils in the United States', *J. Geophys. Res.*, **97**, 7511–7519.

Appendix

The following summarises the changes (from a technical perspective) made to TAPM in going from V2.0 to V3.0.

TAPM V3.0 – Changes from TAPM V2.0

General – Run Pollution from Saved Meteorology

An option has been created to save hourly meteorology to a set of *.m3d files for either all grids, or for only the inner-most grid. The model can then optionally be run again using saved meteorology (reading hourly meteorology back from the *.m3d files, and interpolating in time) in order to decrease overall model run time. In this mode, the model can either be run in a nested pollution mode for all grids, or in a non-nested mode for only the inner-most pollution grid. Pollution options can be modified in the usual way in this mode, although meteorology grids are fixed, giving shorter run times for applications where the same meteorology is needed for multiple pollution runs (e.g. emission scenario modelling, fine-scale pollution modelling), although sub-hourly variations in meteorology are lost in this mode and disk space required to save the *.m3d files may be large for big grids and/or long runs.

The model can now also optionally use a non-centred pollution grid when running the model from saved meteorology in a non-nested mode for only the inner-most pollution grid. This option will allow a user to zoom into an area anywhere on the meteorological grid for fine-scale pollution calculations.

General – Forecasting

A file *_forecast.bat is now automatically created when the *.def file is created, and can be used to run a forecasting application using pre-saved files from TAPM_GUI. It firstly runs a program tapmdata2syng.exe that uses the *.def file and a relative or absolute date input to generate 1) the TAPM synoptic files (*.syn and *.syg); 2) a dates file (*.dates) that TAPM uses to bypass the dates stored in the *.inp file; and 3) a backup.bat file that can be used to store model output in a sub-directory. The *_forecast.bat file then automatically runs TAPM and any other commands that have been inserted into the file to post-process outputs and cleanup/backup files. The *_forecast.bat file can be scheduled to run automatically (e.g. daily) via Windows Scheduled Tasks. Using this forecasting option assumes that a user-defined database of synoptic analyses is available for the dates required.

Meteorology – Maximum Domain Size

Further to the warnings in TAPM_GUI on the maximum domain size allowed, TAPM now stops with an error message if the outer grid domain size exceeds 1500 km in either direction. The synoptic information is also now extracted for a maximum domain extent of 1500 km, consistent with the above limit. Warnings in TAPM_GUI continue to be issued for domain extents larger than 1000 km.

Meteorology – Urban/Industrial Land-use

Extra urban/industrial land-use categories have now been included, and while the default databases do not include these categories, they can be either manually entered or provided to the model via user-defined databases.

Meteorology – Synoptic-scale near-surface wind speed

In order to account for the lowest levels in the synoptic analyses usually being higher than 10 m above the ground, the synoptic wind speed is now adjusted for surface roughness using

a neutral profile with a roughness length of 0.1 m. For LAPS/GASP analyses, this results in the use of a 10 m synoptic wind speed in TAPM of about 70% of the previously used value (which was set to be the same as the value at the first level of the synoptic analyses). This change has had a minimal impact on TAPM predictions (less than 1% decrease in wind speed predictions), as the analyses are only used at the outer grid boundary and to weakly nudge the predictions – TAPM adjusts much more rapidly to the local terrain and land use information than it does to the analyses at 10 m.

Meteorology – Synoptic-scale moisture

In order to account for the lack of cloud water information in the synoptic analyses, we enhance the synoptic total water used in the model, by enhancing the synoptic-scale specific humidity:

$$q_{enhanced} = \max\left(q_{synoptic}, 2q_{synoptic} - q_{sat} RH_C /100\right),$$

where $q_{synoptic}$ is the original synoptic-scale specific humidity and RH_C = 85% is the threshold value above which enhancement is carried out. This parameterisation results in no change to the synoptic-scale relative humidity for $RH_{synoptic} < RH_C$ and gives an enhanced value of 100% when $RH_{synoptic}$ = 92.5%. This approach is consistent with cloud cover parameterisations used in global and synoptic scale models. Note that this formulation is now linear, rather than the overly complex quadratic formulation used in TAPM V2.0.

Meteorology – Ice processes and snow

Ice processes have now been added to the model, including a simple mixed cloud water/ice parameterisation, ice and snow microphysics, and an extra prognostic equation for the specific humidity of snow. Conservation equations are solved for specific humidity (kg kg^{-1}) $q = q_V + q_C + q_I$ (representing the sum of water vapour, cloud water and cloud ice respectively), specific humidity (kg kg^{-1}) of rain water q_R and specific humidity (kg kg^{-1}) of snow q_S. Cloud water and cloud ice are assumed to co-exist only between temperatures of -15°C and 0°C, with a linear relationship used between these two limits (see Rotstayn (1997) for a discussion of mixed-phase clouds). Bulk parameterisations of the micro-physics are based mainly on Tripoli and Cotton (1980) and Lin et al. (1983), with some updated constants/parameterisations as used by Katzfey and Ryan (1997), Rotstayn (1997) and Ryan (2002).

Meteorology – Surface Temperature

The restriction that surface temperature cannot fall below -4ºC has now been removed. The permanent ice/snow land use category has now been set to have a surface temperature of -10ºC rather than being set at the previous minimum surface temperature of -4ºC. The removal of this limit will help to give more realistic sub-zero meteorology in regions where this may be important.

Meteorology – Surface Roughness and Friction Velocity

The surface roughness of soil has been increased from 0.05 m to 0.10 m, in order to attempt to account better for missing roughness effects such as sub-grid-scale terrain and land use effects, which seem to be underestimated with the old minimum value. The vegetation roughness length has also changed to be

$z_{0f} = 0.1 + h_f /10$ ($z_{0f} \le 2$ m), with h_f = Vegetation height (m).

These changes had a moderate effect on predicted meteorology (lower winds speeds for some land use types).

The range of friction velocity has been extended – it can now vary between 0.01 and 2.0 m s^{-1}.

Meteorology – Turbulence

Turbulence kinetic energy and eddy dissipation rate have been enhanced in the top-half of the convective boundary layer (CBL), where previously turbulence levels were underestimated. This has been achieved by using a simple parameterisation that limits the rate of decrease of turbulence with height, between heights in the range 0.55–0.95 times the CBL height. Predicted horizontal and vertical velocity variance and eddy dissipation rate in this region now compare well with CBL observations.

Meteorology – Gravity Waves

The gravity wave time-step has now been linked to the user-selectable maximum synoptic wind speed parameter, similar to the approach used to control the advection time-step. This means that if the maximum synoptic wind speed parameter is selected to be greater than 30 m s^{-1}, then as well as decreasing the advection time-step, the gravity wave time step will also be decreased. This will allow control over the advection and gravity wave time-steps if the model becomes numerically unstable.

Meteorology & Pollution – Horizontal Diffusion

Explicit horizontal diffusion terms were added to the horizontal momentum equations and the equation for virtual potential temperature. This change makes the model more suitable for simulations using high horizontal grid resolution (e.g. ~100 metres) where the current selective horizontal filtering technique (used to eliminate high frequency numerical noise) may not add enough horizontal diffusion in some conditions.

We have now set a minimum horizontal diffusion coefficient for momentum of 10 m^2 s^{-1}, which then gives a minimum horizontal diffusion coefficient for scalars (meteorology and pollution) of 2.5 times this value using the current model formulation. It also translates to a minimum horizontal velocity variance of 0.01 m s^{-1} for LPM pollution mode. These values are consistent with empirically derived dispersion relationships for very stable conditions (e.g. F-Class Stability).

Pollution – Dust Mode

A dust mode has been added that allows pollutant concentration to be calculated for four particle size ranges: PM2.5, PM10, PM20 and PM30. The emissions, background concentrations and output concentrations are relevant for these four categories, while calculations in the model are actually done for: PM2.5, PM10, PM10-20 and PM20-30. This categorisation allows representative particle sizes to be used to account for particle settling and dry/wet deposition. Exponential decay of particles is also allowed, as is available in tracer mode, but there are no chemical transformations or particle growth processes included. The various particle processes used in the model are as for the APM and FPM variables in TAPM V2.0, with some different constants used for the larger size ranges based on Seinfeld and Pandis (1998).

Pollution – Particle settling for APM and FPM

Particle settling for APM and FPM pollutants has now been included, as for dust mode. This will have virtually no effect on APM and FPM concentrations, and was included purely for consistency with the treatment of PM2.5 and PM10 in dust mode.

Pollution – Gridded Surface Emissions

The maximum number of vertical model levels over which gridded surface emissions can be mixed has been increased.

Pollution – Line and Area/Volume Sources

The horizontal increment used to assign line and area/volume sources to the nearest model grid point has been changed from a fixed 10 m to be one-tenth of the pollution horizontal grid spacing. In particular, this change provides faster run-times for simulations with large numbers of large area/volume sources, with no loss of accuracy.

Pollution – Biogenic emissions of nitrogen oxides

Biogenic emissions of nitrogen oxides input into TAPM from the *.bse file are now assumed to be at the standard temperature of 30ºC, with the model now adjusting these emissions using a temperature correction based on Williams et al. (1992):

NO_X, NO_2: $C_T = \exp(0.071(T - 303.15))$,

where T is the soil temperature (K).

Pollution – Chemistry Mode

The deposition constants for nitrogen dioxide have been modified to be

NO_2: $r_{water} = 1500, r_{soil} = 500, Sc = \sqrt{46/18}$,

which now allows a more realistic contrast between water and soil surfaces.

Pollution Output File (.glc)*

The pollution output file format has been modified to store ground level concentrations as real numbers rather than as 2-byte integers. Pollution output is now stored in *.glcr files rather than the old *.glc files – note that backwards compatibility with *.glc files has been maintained.

Pollution – Concentration Output in 3-d

Three-dimensional concentration fields can now optionally be output to files (*.c3d).

Deposition in Tracer Mode

Optional deposition (dry and wet) has been added to the Tracer Mode in the model. A number of species with non-zero deposition characteristics can be selected individually for each tracer, with dry deposition characteristics:

SO_2: $r_{water} = 0, r_{soil} = 1000, Sc = \sqrt{64/18}$;

HF: $r_{water} = 0, r_{soil} = 100, Sc = \sqrt{20/18}$.

Both of these species are assumed to be readily dissolved in water, and so totally removed by wet deposition. This assumption for sulfur dioxide is different to that used in chemistry mode, as other species needed to calculate the amount dissolved in the available liquid water (e.g. hydrogen peroxide and ozone) are not available in tracer mode.

Pollution – Concentration Variance

A new pollution option has been created to calculate concentration variance $\overline{\chi'^2}$ in Tracer Mode, and for sulfur dioxide in Chemistry Mode. Output files for concentration variance on the pollution grid are now output into files (*.glcv), and, if available, are read by various pollution post-processing utilities.

Pollution – Peak-to-Mean Concentration Statistics

The calculation of peak-to-mean concentration is now done when pollution is post-processed. The maximum hourly-averaged concentration is enhanced to obtain peak concentration estimates for 10-minute, 3-minute, 1-minute and 1-second averaging periods. Peak concentrations are calculated using the commonly used power-law relationship, but with an exponent that depends on concentration fluctuation intensity I_C (derived from the mean and variance of the concentration output from the model):

$$C_{MAX}(t) = C_{MAX}(3600)\left(\frac{3600}{t}\right)^{\min\left(0.1+0.25I_C^{1/3},0.4\right)},$$

with *t* the averaging period (s), and

$$I_C = \left(\frac{\overline{\chi'^2}}{\overline{\chi}^2}\right)^{1/2}.$$

Note that the peak-to-mean approach is only valid for long time-series, and is typically used for results from annual model runs.

Pollution – Building Wakes

The effect of building wakes on plume rise (EGM and LPM modes) and on point source dispersion (LPM mode) was included in TAPM V2.0. The influence of building wakes on dispersion in EGM mode has now also been implemented, and will allow building wake effects to be included not only for point sources, but also for line, area/volume and gridded emission sources. The approach taken is to modify the mean and turbulence fields from those predicted with the meteorological module, by using the same corrections for building wake meteorology and turbulence, based on the PRIME parameterisations, that were implemented previously.

The constant $i_{zc} = 1.00$ has been modified to be $i_{zc} = 0.65$ to give a slightly improved comparison against laboratory experiments for the cavity region in LPM mode.

Pollution – Concentration Background File

An optional concentration background file (*.cbg) can now be provided by the user that contains hourly concentration for six species. If this file is available, it is used as inflow boundary conditions for the outer-most model grid. If *.m3d files are being used to run the inner-most grid only, then the *.cbg file will be used to provide boundary conditions for this grid.

Note that nitrogen dioxide background concentration is set equal to the nitrogen oxides background concentration, as is normally done for non-time-varying background concentration (available in the GUI).

Pollution – Dust Mode Wet Deposition

The wet deposition algorithm in Dust Mode had previously used total liquid water (cloud plus rain) to determine the amount of pollution to be rained-out, whereas it should have been only the rain water fraction – this has now been corrected.

Pollution – Point Sources

The option to switch-off a point source by setting the mode to -1 in the point source emission file, while working for the inner-most grid, was setting the mode to 0 by mistake (EGM mode) for outer grids. This could cause erroneous results on outer grids, and could also cause problems with the inner-most grid boundary conditions – this error has now been corrected.

Pollution – LPM Mode Only

When the off-line meteorology option (using *.m3d files) is used for the inner grid only, then an option to use only LPM mode (no EGM calculations) for sources in this mode, is now available. This option will allow simulations to be made in LPM mode without the overhead of running the EGM grid, thus speeding-up simulations. In this mode there is no conversion of pollutant mass to the EGM grid after a certain travel time, and no chemistry, deposition or particle settling. In tracer mode, exponential decay is still available.